Development of an innovative interfacial layer adapted to La2BO4±δ (B: Ni, Mn, Co) IT-SOC oxygen electrodes

Sabah Amira, Mosbah Ferkhi, A. Khaled, Fabrice Mauvy, Jean-Marc. Bassat, Michel Cassir, Jean-Claude Grenier

Development of an innovative interfacial layer adapted to $La_2BO_{4\pm\delta}$ (B: Ni, Mn, Co) IT-SOC oxygen electrodes

S. Amira[1,2], M. Ferkhi[1,2,4*], A. Khaled[1], F. Mauvy[4], J. M. Bassat[4], M. Cassir[3], J. C. Grenier[4]

[1] Département de Chimie, Faculté des Sciences Exactes et Informatique, Université Mohamed Seddik Ben Yahia, BP98 Ouled Aissa, 18000 Jijel, Algeria.

[2] Laboratoire d'Etude sur les Interactions Matériaux-Environnement (LIME), Université Mohamed Seddik Ben Yahia, BP98 Ouled Aissa, 18000 Jijel, Algeria.

[3] PSL Research University. Chimie ParisTech, IRCP, I2E, 11 rue Pierre et Marie Curie, 75005.

[4]CNRS, Univ. Bordeaux, Bordeaux INP, ICMCB, UMR 5026, F-33600 PESSAC Cedex, France

Abstract

An architectured interlayer composed of 50 % YSZ ($(ZrO_2)_{0.92}(Y_2O_3)_{0.08}$) and 50% GDC ($Ce_{0.90}Gd_{0.10}O_{1.95}$) (so-**c**alled YSZ+GDC) was successfully layered between the YSZ electrolyte and the $La_2BO_{4\pm\delta}$ (B: Ni, Mn, Co) oxygen electrode materials with the aim to improve the electrochemical performance of the corresponding Intermediate Temperature-Solid Oxide Cells (IT-SOCs). Various physical and chemical characterizations were carried out to assess the purity of the materials and the chemical reactivity between the different constituents of the electrochemical cell. The oxygen electrode performance was carried out by Electrochemical Impedance Spectroscopy (EIS) measurements. $La_2NiO_{4\pm\delta}$ material in the presence of this interfacial layer (YSZ+GDC) and YSZ as electrolyte shows the lower ASRs values: 0.43 and 0.18 Ω.cm² at 600 and 700 °C, respectively. Moreover, this architectured electrode shows a quite low activation energy value of the ASR, that is of the order of 0.72 eV. This remarkable behavior enables us to propose this design as an alternative oxygen electrode for IT-SOC with a specific (YSZ+GDC) composite film as interfacial layer between cathode and YSZ electrolyte.

Keywords: Interfacial Layer, Ruddlesden-Popper oxides, Solid Oxide Fuel Cells (SOFC), Mixed Ionic and Electronic Conductors (MIEC), Area Specific Resistances (ASR).

1. Introduction

It has become clear that SOFC systems, which are electrochemical systems, can become alternatives in the field of renewable and sustainable energy, thus solving the problems of environmental pollution and ensuring clean and efficient energy conversion [1]. Despite this, the commercialization of SOFC cells is still limited and has not yet been completely achieved. One of the solutions is the development of new architectures of cells, which can resolve several problems of the SOFCs, reducing the working temperature towards so-called intermediate temperatures of approximately 600 °C, and increasing the lifetime.

The field of materials and their applications has recently experienced remarkable development, particularly with regard to both Solid Oxide Fuel Cells (SOFCs) and Solid Oxide Electrolysis Cells (SOECs) in order to develop their performance and reduce the problems associated with high-temperature operation (≈ 700-800 °C). One of the current research challenges is the optimization of oxygen electrode materials with a high mixed electronic and ionic conduction, a high electrocatalytic activity ensuring the fast exchange of oxygen and a porous morphology allowing a sufficient surface area. In addition, during their operation, and under working conditions, such active materials must have **good** chemical stability with respect to the electrolyte, in particular at high **temperatures**, avoiding the formation of secondary and blocking phases at the interface.

The A_2BO_4 oxide family is of particular interest in the case of electrochemical energy applications such as described above **b**ecause their oxygen surface exchange kinetics and oxygen diffusion are higher than those of the more usual ABO_3 oxides **[2]**. Due to the adjustment of two different structural units, the A_2BO_4 structure can be appropriately described as a succession of sheets of BO_2 square planes and A_2O_2 layers of the NaCl-type **[3]**. The ionic conductivity of these materials results from the oxygen excess δ housed in their A_2O_2 layers involving the apical oxygen atoms (interstitia**lly** mechanism) **[4-6].** These interstitial atoms are highly mobile, which induces a high ionic conductivity of the material. The mixed valence of the transition metal, B^{2+}/B^{3+}, results in a sufficiently high electronic conductivity for the application, even if lower than those of perovskites. **Moreover, one of the interesting properties of these materials is the values of thermal expansion coefficients (TEC) which are close to those of classical SOFC electrolyte materials, such as doped ceria and stabilized zirconia oxides [7- 10].**

Much of the initial works on these phases focused on the $Ln_2NiO_{4+\delta}$ compounds, where Ln: La, Pr, Nd, Sm **[10, 11]**. The presence of several valence states of cobalt (Co) and manganese (Mn)

can provide the cobaltite and manganite material with interesting electrochemical properties **[12].** To date, undoped lanthanum manganites and cobaltites (La_2MnO_4 and La_2CoO_4) oxides used as cathode materials for SOFCs have not been studied and the electrochemical properties have not been detailed. Investigations have been focused on other materials of the A_2BO_4 type, in which A is an atom of Sm or Pr and B is Mn or Co. For example, at temperatures of 600 and 700 °C, S. Liping *et al*. **[12]** have shown that by increasing the rate of site substitution of lanthanum by strontium in $La_xSr_{2-x}MnO_{4+\delta}$ materials, the values of ASRs increase by a factor of 2. The values of the activation energies follow the same tendency. These authors also showed that no reaction occurred between $La_xSr_{2-x}MnO_{4+\delta}$ and GDC at an annealing temperature of 1000 °C.

As for cobaltite materials A_2CoO_4 (A: Pr or Sm), Y. Wang *et al.* **[13]** showed that the Thermal Expansion Coefficients **(TECs)** of cobalti**t**e materials are much higher than those of ferrites. The electrical conductivity of cobaltites is in the order of 10^2 S. cm^{-1} close to 800 °C, which is satisfying for the IT-SOFC cathode.

However, several groups studied unsubstituted materials: Bassat *et al.* **[2]** and Skinner *et al.* **[6]** found fast oxide ion conductivity over a wide temperature range indicating a high potential for use as oxygen electrode material in SOC cells. According to the literature, substitution with high-valence cations, such as Fe, Mn or Co ions at Ni sites in La_2NiO_4 can **influence significantly the oxygen ionic transport [5].**

Previous studies have shown promising performances of these nickelates with various electrolyte materials. It has been observed that $Nd_2NiO_{4+\delta}$ shows a low reactivity with respect to YSZ and has interesting properties under polarization **[7]**. Philippeau *et al.* **[14]** have studied different materials in the presence of GDC and LSGM as electrolytes; such materials show low polarization resistances at 600 °C, around 0.28 Ω.cm^2. For $La_2NiO_{4+\delta}$ and $Pr_2NiO_{4+\delta}$ materials, the ASR values were 0.93 Ω cm^2 and 0.15 Ω cm^2 at 600 °C, respectively.

Recently, D. Kim *et al.* [10] also investigated ORR activity and durability of $Ln_2NiO_{4+\delta}$-YSZ (Ln: La, Nd, and Pr) composite cathodes, and they have concluded that these two properties strongly depend on the A-site lanthanides.

According to Lu *et al.* [15], a mixture composed of $La_2NiO_{4\pm\delta}$ with $LaNiO_3$ can significantly improve the performance of SOFCs. In addition, T. Chiu *et al.* [16] showed that a cathode composed of 40 wt% $LaNiO_3$ exhibited the lowest polarization resistance at 700 °C in air.

In order to improve the electrochemical performance of SOFC cells operating at intermediate temperatures (IT-SOFC) by avoiding all the problems related to the chemical reactivity between

the electrolyte and the other constituents of the cell, new architectures on the electrolyte side have been developed **[17-18]**. In order to obtain highly active cathode materials, Mohebbi *et al.* **[19]** prepared bilayers based on YSZ/GDC in the form of thin layers using the flash sintering method. In this case, the fabricated single SOFC cell made using bilayer YSZ/GDC electrolyte shows a performance of 0.3 W/cm^2 at 800°C, about 15% higher than the SOFC single cell made by conventionally sintered YSZ/ GDC electrolyte. Furthermore, the optimized cell yields a promising electrochemical performance of 1.45 W/cm^2 at a current density of 2 A/cm^2 and low ohmic resistance of 0.046 **Ω** cm^2 at 800 °C.

The interfacial layer contributes at the same time to the improvement of the mechanical adhesion and electrochemical properties by improving the ionic transfer and reducing the electrode overpotentials **[20]**. It makes **it** possible to block the diffusion of cationic species at the level of the "diffusion barrier" interface, which prevents the occurrence of secondary insulating phases. For instance. Ogier *et al.* **[20]** found that the presence of a $Ce_{0.8}Gd_{0.2}O_{2-\delta}$ (GDC) layer or $Ce_{0.72}Y_{0.18}O_{2-\delta}$ (YDC) layer located between the oxygen electrode materials ($La_{0.6}Sr_{0.4}Fe_{0.8}Co_{0.2}O_{3-\delta}$, $La_2NiO_{4+\delta}$, $Pr_2NiO_{4+\delta}$, $Nd_2NiO_{4+\delta}$) and 8YSZ electrolyte significantly reduces the oxygen reaction resistances.

An important enhancement of the total ionic conductivity with decreasing crystallite size was observed, assigned to an almost ideal parallel connection between both nanophases, coupled to an increase of their grain boundary ionic diffusivity. In addition, it was proved that the presence of the YSZ phase significantly improves the mechanical properties of the cell. **In a recently published work by Ferkhi *et al.* [21], the introduction of a composite layer consisting of 50% YSZ+ 50% GDC between the GDC and a $La_{1.5}Pr_{0.2}Nd_{0.3}NiO_{4\pm\delta}$ (LNPNO5) material contributes, significantly, to improving the electrochemical performance of such a cell by leading to lowest ASR values of the electrodes (0.06 Ω. cm^2 at 700 °C and 0.022 Ω. cm^2 at 600 °C). The improvement of these performances is due to the creation of additional conduction sites (Oxygen Vacancies) by the addition of Pr and Nd elements in the LNPNO5 and to the presence of this layer which contributes to the improvement of the mechanical properties and to the participation to avoid of any chemical reaction between the components of the cell.**

Based on the information mentioned above and with the aim of improving the electrochemical performances of SOFCs at the oxygen side, an innovative interfacial layer composed of 50 % YSZ and 50 % GDC (YSZ+GDC) in mass was introduced between typical oxygen electrode materials ($La_2NiO_{4+\delta}$, $La_2MnO_{4+\delta}$ and $La_2CoO_{4+\delta}$) and the YSZ electrolyte. The chemical reactivity between these compounds and the electrolyte was first studied using X-ray

Diffraction (XRD) analyses. The oxygen over-stoichiometry was determined by iodometry. SEM analyses of the cells were performed in order to examine their microstructure and grains morphology. XPS analysis was carried out to study the elemental surface composition and the oxidation states of the various elements constituting the surface of the as-prepared materials. Then, after shaping the electrodes, Electrochemical Impedance Spectroscopy (EIS) measurements were carried out with the aim of characterizing the electrochemical performances and identifying the different contributions to the polarization resistance as well as the limiting step of the Oxygen Reduction Reaction (ORR) process under SOFC mode and Oxygen Release Reaction (reverse process, *i.e.* under SOEC mode).

2. Experimental

2.1. Preparation and characterization of oxygen electrode materials

Oxygen electrode materials were prepared by the citrate method which was previously described in detail by Ferkhi *et al.* **[22, 23]**, the synthesis protocol was as follows: it consists first of all in dissolving the metal nitrates (*i.e.*. ($Ni(NO_3)_2.6H_2O$, Sigma-Aldrich, 97.0%), manganese ($Mn(NO_3)_2.6H_2O$, Sigma-Aldrich, 99.9%) and cobalt ($Co(NO_3)_2.6H_2O$, Sigma-Aldrich, 98.0%)) in water. The solubility of these three nitrates being high, only the La_2O_3 oxide was dissolved in nitric acid in adequate quantity. The obtained aqueous solutions were mixed and the citric acid was added in a second step. The mixture was heated to approximately 75 °C, with moderate stirring. The viscous gel formed was dried at less than 120 °C and the powder **calcined** as follows: 175 °C for 1 hour, then 350 °C and 500 °C for 1 hour to eliminate the nitrates and all the remaining organic matter, respectively. The final **sintering** was carried out at 1000 °C in **the** air for 4 hours.

The phase purity was checked by X-ray diffraction. The data were collected at room temperature over the 2θ angle range 20–80° with a step of 0.02° using **an** XPERT-PRO powder diffractometer in the Bragg–Brentano geometry using the CuKα radiation (λ = 1.5406 Å).

The reactivity test between YSZ and GDC electrolyte was carried out under 1350 °C for 3 days and at 1000 °C between electrodes La2BO4 (B: Ni, Co or Mn) and YSZ+GDC for 3 days.

XPS measurements were carried out on a Thermo Fisher K-Alpha spectrometer using a monochromatic Al Kα X-ray beam (1486.6 eV, 300 µm spot size) equipped with a hemispherical deflector analyzer operating at constant energy. A 300 µm diameter X-ray beam spot was used. Surface charge effects were avoided using an electron flood **g**un. The

pressure in the analyzer chamber was 2 x 10^{-8} Pa. The survey spectra were recorded with a pass energy of 200 eV and, for higher resolution, this energy was lowered to 30 eV. The Thermo Scientific Advantage software (version 5.943) was used for collecting and processing the spectra. Binding energy shifts were calibrated against the adventitious position of the C1s carbon set at 284.6 eV and the BE precision was ± 0.1 eV.

The morphology and microstructure of the powders and pellets were studied using a JEOL / EO version 1.07 Scanning Electron Microscope (SEM). From the cross-section of the cell, the cathode layer thickness was measured as well as the porosity calculated by means of image analysis (Image J software).

The values of the oxygen over-stoichiometry δ were determined through iodometric titration. This analytical method is well known and extensively described for instance in ref. **[24].** The dosage was performed under agitation, heating at 60 °C until the oxide dissolves completely; an important parameter is that an argon flow was used to prevent the oxidation of I^-.

2.2. Preparation of dense electrolytes and interfacial layer. Electrochemical Measurements.

The shaping of YSZ electrolyte dense pellets was carried out by Isostatic Pressing (IP) performed at 3000 bars for 5 min; the obtained pellets were then sintered for 10 h at 1400 °C. The thickness and the diameter of the pellet are 1.5 mm and 1.6 cm respectively. In order to elaborate the symmetrical half cells, the interfacial layer was deposited by painting on both surfaces of an YSZ pellet. For this purpose, a mixture of YSZ and GDC (50 – 50 wt %) was prepared in a methyl cellulose solvent (**Fig.1**). A sintering treatment at 1350 °C **for** 1 hour is necessary to **ensure** good adhesion of this interfacial layer on the electrolyte pellet.

The ionic conductivity of the YSZ electrolyte support and of the interfacial layer (YSZ+GDC), as well as the polarization resistance of the cathode materials were measured by EIS. These measurements were performed in a two-electrode configuration (under zero d.c. conditions) on a symmetrical cell, using an Autolab PGSTAT 30 in the range of 0.01 Hz to 1 MHz with a 50 mV signal amplitude. The complex impedance diagrams were analyzed by means of the Zview™ software using various equivalent circuits constituted of R-CPE elements, associated in parallel.

3. Results and Discussion

3.1.Structural characterization

The XRD patterns of the different synthetized compounds, $La_2NiO_{4+\delta}$ (L2NO), $La_2CoO_{4+\delta}$ (L2CO) and $La_2MnO_{4+\delta}$ (L2MO) are characteristic of single phases without traces of impurities **(Fig.2)**. The L2MO material crystallizes according to a tetragonal structure of high symmetry (I4/mmm space group (JCPDS # 33-0897)). Both oxides, L2NO (JCPD # 21-1274) and L2CO (JCPD # 43-1081) **c**rystallize according to the expected orthorhombic structure (Fmmm space group) **[22, 23, 25-28]. The averages crystallites sizes of different oxides were calculated using Debye-Scherer's formula, as shown in Equation (1):**

$$\boldsymbol{D = \frac{0.9\,\lambda}{\beta \cos\theta}} \text{ .....(1)}$$

The calculated values are: for L2NO and L2CO are ~48 nm and 35 nm, and for L2MO is ~41 nm. The refined unit cell parameters are summarized in Table 1.

It is interesting to notice that occupying the B site of the A_2BO_4 structure with manganese ions reduces the structural stresses, resulting in a higher crystal structure symmetry, keeping the cell undistorted. This also explains the decrease in lattice parameters and volume compared to nickel and cobalt-based materials.

3.2.XPS Analysis

The XPS spectra recorded for the O1s, Ni $2p_{3/2}$, Co $2p_{3/2}$, Mn $2p_{1/2}$ and La $3d_{3/2}$ core-level peaks are reported in **Figure 3** and **Table 2**. The O 1s peaks of the L2NO, L2CO and L2MO materials show a complex shape leading to a decomposition into four peaks for L2NO and L2MO and five peaks for L2CO (**Fig.3.a,c,e**). This multiplicity may be due to the difference in nature of the metallic elements associated with the oxygen anions. **The** low **binding** energy peaks (1) and (2) located in the range **of** (528.52 - 528.69) eV and (529 , 66 - 530.13) eV respectively, represent the oxygen anions of the crystal lattice **[29, 30]**; peak (3) **which is located** at (531.14 - 531.45) eV can be attributed to the metal hydroxyl and the carbonate groups **[31, 32]**. **This is** because rare-earth oxides are very hygroscopic and easily carbonated when they exposed to atmospheric conditions **[33]. The** last peaks at the highest **binding energies** (4 and 5) **are** probably result from adsorbed molecular water **[34].**

Figure 3.f shows the two regions of La $3d_{3/2}$ and Ni $2p_{3/2}$, and differentiating between them is somewhat difficult. However based on the previous studies we can say that the two peaks observed in th low binding energies at 849.94 eV and 851.58 eV can be attributed to lanthanum La$3d_{3/2}$ **compoenents [35,36]** while the last two high energy peaks located at 854.43 eV and 855.7 eV correspond to Ni (II) and Ni (III), respectively **[36,37]**. In addition, analysis of peak

deconvolution of Co $2p_{3/2}$ **(Fig.3.d)** results in two peaks located in the intervals [779.14-779.63] and [780.37-781.07] eV attributed to Co **(III)** and Co **(II)**, respectively **[37, 38].**

The high resolution spectrum of Mn 2p of the L2MO material shows two main peaks located at 641.30 **eV** and 652.91 eV separated by a value of 11.61 eV due to spin-orbit coupling and which are attributed to Mn $2p_{3/2}$ and Mn $2p_{1/2}$, respectively. The decomposition of these two peaks results in four components: at 641.12 and 652.69 eV, corresponding to the binding energy of Mn^{3+}, while the others at 642.61 and 655.49 eV are attributed to the energy of Mn^{4+} binding agent **[39- 41], (Fig.3.b).**

The atomic ratios of the different elements were also calculated and summarized in **Table 3.** Lanthanum is present on the surface in large quantities and is more widespread compared to nickel in the case of LMO materials.

The atomic ratios of elements **at the surface of** all materials were determined by XPS and summarized in **Table 3.** The results show that the lattice oxygen content at the surface (O_{latt}/Σcations) is slightly higher than that of the bulk, indicating an anionic character of the surface of L2BO materials. This may provoke a higher surface activity of the materials. On the other hand, due to the coexistence of Ni(II) and Ni(III), Co(II) and Co(III) as well as Mn(III) and Mn(IV) on the surface of L2NO, L2CO and L2MO materials, respectively, the cationic redox reaction, surface charge storage as well as electronic and ionic properties can also be improved **[39].**

Generally, the surface state can influence, either positively or negatively, the phenomenon of adsorption of oxygen molecules on the surface of materials by favoring or disfavoring this phenomenon. In addition, in such layered materials, it is of high interest to probe the outermost atomic layer to learn about their surface termination, in order to determine whether it is a transition metal (here Ni) or (Ln/Sr) cations. This information is indeed very important with respect to the oxygen reduction processes. A lot of work has been performed by the group at Imperial College London, either regarding Co-based perovskites and nickelates such as those studied in this work **[42, 43]**. For this purpose**,** the authors combined LEIS (Low Energy Ion Scattering) and XPS experiments. They have demonstrated by LEIS that the outermost surface is in fact Ln/Sr terminated. In complement, angle-resolved XPS measurements lead to **obtaining** a compositional depth-profile. Clearly**,** the amount of Ni decreases as the surface is approached, in good agreement with LEIS results. In close relation **to** this result, the authors proposed the existence of surface oxygen vacancies, which are also in good agreement with thermodynamic calculations. This conclusion has to be put in relation to our own results obtained by XPS.

3.3.Oxygen stoichiometry (δ) and iodometric titration

The over-stoichiometry δ values obtained by iodometric titration for the as-prepared materials are reported in Table SI1. The excess oxygen in $La_2NiO_{4+\delta}$ is 0.177 at room temperature, which agrees with values reported by several authors who used a similar synthesis procedure. This is also consistent with the thermal behavior observed in TGA experiments **[44-48]**. For $La_2CoO_{4+\delta}$, the δ value (δ = 0.248) is larger than those of the nickelate, cuprate, and even the lanthanum manganite **[49]**. According to the work of Le Toquin *et al.* **[50]** carried out on single crystals of $La_2CoO_{4+\delta}$, the δ value ranges from 0.09 to 0.20, while Yu. Huan *et al.* **[3]** found the highest value, δ ~ 0.46 in an oxidizing atmosphere. Compounds containing manganese are particularly interesting because in such A_2BO_4-type structure, manganese can have various oxidation degrees (+ II), (+ III) and (+ IV), which gives a wide range of oxygen stoichiometry. Indeed, both an oxygen deficit and an over-stoichiometry can be tuned thanks to the change of the B element in the La_2BO_4 structure **[51, 52]**. In our case, a value of δ ~ 0.13 was observed at room temperature for $La_2MnO_{4+\delta}$, which corresponds to a mixed valence Mn^{2+}/Mn^{3+}.

3.4. Scanning Electron Microscopy

SEM images recorded on the painted electrodes for each material are reported in Figure 4. It is observed that the materials have different porosity. L2NO is much more porous compared to L2MO and L2CO materials which, probably, improves its catalytic and even electrocatalytic properties by increasing the specific surface. The grains of the materials are homogeneous and of the same size with a spherical shape.

SEM images recorded for the cross-sections of symmetrical cells **(Figure 5)** clearly show that the interfacial layer is homogeneous and well adherent to the electrolyte and to the oxygen electrode materials, no signs of reactivity were observed at the interfaces**.** It is expected that this good adhesion may lead to a larger contact area and hence lower the interface resistance, inducing an improvement of the electrochemical reactions.

3.5. Chemical Reactivity

The chemical reactivity between the different constituents of the symmetrical half-cells was carried out on the various YSZ and GDC electrolyte powders mixtures for 3 days at a fixed

temperature of 1350 °C. **Figures 6, 7 and 8** show the XRD diffractograms after thermal treatments (IL: (YSZ+GDC), (IL/YSZ, IL/GDC), and L2NO/IL.

The reactivity test between the two electrolytes (**Figure 6**) shows that both compounds (YSZ, GDC) preserve their structure after a long annealing treatment at high temperature. Only the peaks characteristic of the two phases (YSZ, GDC) appear **[14, 20]**. Obviously, no additional peaks can be identified in XRD diffractograms, indicating that no chemical reaction occurred. Similarly, the diffractograms reported in **Figure 7** show no significant reactivity between both the electrolytes and the interfacial layer. Once more, no supplementary peaks characteristic of a new phase were detected.

However, it is important to recall that YSZ and GDC can chemically react, leading to the formation of a solid solution, mainly above 1000°C and during a long dwell time **[53]**. The corresponding formed oxides remain ionic conductors even if their conductivity is lowered compared to those of the YSZ and GDC parent oxides **[54]**. Therefore, for the current work it was useful to check the chemical reactivity between the two components of the composite interfacial layer.

The thermal treatment of powder mixtures of L2NO, L2MO or L2CO electrode materials with the (YSZ+GDC) interfacial layer performed at 1000 °C for 3 days in air, did not result in the formation of undesirable phases and show no significant decomposition. These results indicate that L2NO, L2MO and L2CO electrode materials seem chemically stable and compatible with the interfacial layer used. The XRD pattern of L2NO is reported in Figure 8. The same remark was given by Ferkhi *et.al* **[22,23]**, but such observations appear in contradiction with previous literature data reported by Philippeau. *et al.* **[14]**. Indeed these authors reported the complete decomposition of the La_2NiO_4 phase into the Ruddlesden Popper $La_4Ni_3O_{10}$ phase after heating at 1150 ° C for 1 h with the GDC electrolyte. The same behavior was observed by Montenegro-Hernandez *et al.* **[7]** during the study of La_2NiO_4 /CGO, $LaNiO_3$ and $La_4Ni_3O_{10}$ phases, obtained after heating in air at 900 °C for 72 h. Several studies carried out on lanthanum nickelates as cathode for SOFCs have reported the formation of an insulating and blocking layer based on lanthanum zirconate $La_2Zr_2O_7$ at the LNO / YSZ interface resulting from the diffusion of cations towards the cathode / electrolyte interface **[7, 55]**.

Compared to the previously published results and on the basis of the chemical reactivity tests performed in this work, in which no other phase has been detected, the proposed interfacial layer has a positive influence in terms of chemical stability, not only in the low SOFCs operating temperature range **[14]**, but also in higher temperature range (1000 °C). It can be deduced that

this layer prevents any reactivity between the oxygen electrode and the YSZ and GDC electrolytes.

3.6. Electrochemical measurements

In order to evaluate the electrochemical performances of the studied oxygen electrodes and the role of the interfacial layer, EIS measurements were carried out in a temperature range between 300 and 750 °C.

First, the YSZ electrolyte was characterized: a single phase YSZ pellet covered on both sides with a platinum ink was used as a reference sample. EIS measurements were performed before studying the contribution of the interfacial layer. **Figure 9** shows a typical example of a corresponding Nyquist diagram recorded at 400 °C for a Pt/YSZ/Pt symmetrical cell. Two semi-circles appear at high (HF) and medium (MF) frequencies, located between 1MHz to 60 KHz and 60 KHz to 10 Hz; they correspond to the response of the bulk material and grain boundaries, respectively. **The data from the EIS analyses were fitted to the equivalent circuit of the (R1//CPE1)-(R2//CPE2) type (as described in the inset of Figure 9).** The corresponding Arrhenius diagram of the ionic conductivity is reported in **Figure 10 ;** for comparison the results found by Philippeau *et. al* **[14]** are also reported**.** The associated activation energy is close to 0.95 eV and in good agreement with literature data **[53]**.
Then, the symmetrical cell (Pt//(YSZ+GDC)//YSZ//'(YSZ+GDC)//Pt including the interfacial (YSZ+GDC) layer previously described and deposited on the YSZ electrolyte was studied. The Nyquist diagrams, as well as the used equivalent circuits, recorded at various temperatures (300, 400 and 700 °C) are plotted in **Figure 11**. The Nyquist plots show a high frequencies (HF) > 10^3 Hz contribution, attributed to the YSZ electrolyte response. The HF depressed semi-circle can be decomposed into two semi-circles, modeled by equivalent circuits composed of two parallel R-CPE elements connected in series at 300 °C, and by R and two R-CPE elements connected in series at 400 °C. The two semi-circles characterize the YSZ electrolyte, the first (HF1) can be assigned to the bulk contribution and the second (HF2) corresponds to the grain boundaries response.
Both impedance contributions are clearly distinguished in the temperature range around 300 °C (see **Figure 11**). According to what has been previously published [**22,23**], the resistances are inversely proportional to the temperature, and the high frequency semicircles relative to the bulk and the grain boundaries tend to be progressively less visible and disappear at high temperatures **(700 °C)** . Therefore, by comparison with the YSZ electrolyte response at 400 °C

(see **Figure 9**), and according to the equivalent circuits shown in the figure, we can confirm that the medium frequencies (MF) semi-circles observed between 10^4 and 100 Hz can be assigned to the response of the (YSZ + GDC) interfacial layer; such a contribution is well separated from that of the YSZ electrolyte in the temperature range 400 - 700 °C (**Figure 11**). The low frequency impedances (between 100 - 10^{-2} Hz) have been attributed to the contribution of the electrode reaction as commonly mentioned in the literature **[56]**.

The Arrhenius plots of the interfacial layer ionic conductivity as a function of the inverse of temperature is shown in **Figure 12**. The conductivities of YSZ and the YSZ-GDC interfacial layer were calculated using the following relation **(2)**:

$$\sigma = \frac{1}{R}\frac{e}{S} \quad \text{.....(2)}$$

where:

R: Electrolyte or interfacial layer resistance,

e: Thickness of YSZ pellet and IL,

S: Surface of YSZ pellet.

For comparison, the ionic conductivity of the whole interfacial layer and YSZ at 700 °C is of 30.9 $mS.cm^{-1}$, which is a rather acceptable value for an interfacial layer at intermediate temperatures **[57]**.

Finally, the influence of the interface layer on the electrochemical performance of the symmetrical cells (cathode / interfacial layer / electrolyte / interfacial layer / cathode) has also been studied. The electrochemical properties of the ORR using L2NO, L2MO and L2CO as oxygen electrode materials were investigated by measuring the polarization resistances. Typical Nyquist diagrams of the symmetrical cell L2NO / YSZ+GDC / YSZ/L2NO are reported in **Figure 13**.

The EIS diagrams can be decomposed **into** three main parts and associated electrochemical processes can be proposed based on previous**ly** reported data **[58]**:

- ***The ionic conduction process at the electrolyte level***: this process appears at high frequencies, expressed by the conduction of O^{2-} ions in the bulk (HF1 > 10^5Hz) and the grain boundaries (10^5 > HF2 > 10^3 Hz), expressed by the two HF semi-circles (**Figure 13**) evidenced in the low temperature range (around 300 °C). These two contributions gradually disappear with the increase in temperature.
- ***The ionic transfer process at the interfacial layer***: this impedance contribution can be expressed by a depressed semi-circle located in the medium frequency (MF) range (10^4 – 100 Hz), characterizing the ionic transfer and the response of the interfacial layer

(YSZ+GDC). It can be therefore mainly assigned to the O^{2-} ions conduction through the interfacial layer. This impedance contribution is similar to the one corresponding to the interfacial layer deposited alone on the single phase YSZ electrolyte, which can be observed in the same frequency range (**Figure 11**) at 400 °C.

- ***The ORR process at the oxygen electrode material***: observed in the two LF semi-circles (at lower frequencies 10^{3}-10^{-2} Hz), this impedance contribution is related to electrode reactions (adsorption-desorption, dissociation, charge transfer and O_2 gas diffusion of through the pores of the electrode).

The Area Specific Resistances (ASR, in Ω.cm^2) of the L2NO, L2MO and L2CO cathodes materials were deduced from the polarization resistance (Rp) using the following relation **(3)**:

$$\boldsymbol{ASR = \frac{R_p}{S} \times 2} \quad \text{.....(3)}$$

where R_p is the electrode polarization resistance corresponding to the addition of the real parts of the last two half-circles (in ohm) and S, the geometrical surface (in cm^2).

Figure 14 shows the Arrhenius plots of the ASR of the L2NO, L2MO and L2CO oxygen electrode materials deposited on the YSZ electrolyte in the presence of the (YSZ+GDC) interface layer. It is interesting to compare these values to previous results reported in **Table 4**. It can be clearly seen that the addition of this interfacial layer between the oxygen electrode and the YSZ electrolyte induces a significant drop in the ASR and reduces the activation energy.

All the single phase materials based on nickelate, manganate or cobaltite lanthanum oxides, developed and studied until now for SOFCs cathodes, have higher values than the selected materials presented in the present study when combined with an optimized interfacial layer composed by YSZ + GDC mixture.

With the exception of L2CO material, based on the results of surface analysis, oxygen over-stoichiometry, SEM micrograph and electrochemical properties (**Table 4**), it can be concluded that the improvement of the electrochemical properties of the selected cathodes materials by adding an interfacial layer shows the interest of using such rare-earth oxides combined with (YSZ+GDC) interfacial layer for IT-SOCFs. **The improvement of the electrochemical performance of the cited materials may be due to the increment of their surface oxygen vacancies, which result in a faster ion mobility and improvement of catalytic activities at the cathode side. Surface oxygen vacancies play a key role for reducing the electrode polarization resistance.. Another reason could be the improved ionic conductivity due to the addition of ionic conductor YSZ+GDC as an interface between cathode and YSZ, which significantly improves the ionic transfer. As a result, the electrocatalytic**

functionalities get faster and electrode polarization values reduce in the fabricated L2NO and L2MO cathodes [63, 64].

The equivalent capacitances (CPE) of each impedance contribution are plotted as a function of temperature using **Schouler's** method **[59, 60]** in **Figure 15**. Nevertheless, the attribution of chemical and / or electrochemical processes is not straightforward.

The capacitance values of the medium frequency (MF) contribution are between $5*10^{-5}$ and $2*10^{-4}$ F.cm^{-2} ascribed to the grain (G) and grain boundary (GB) response of the electrolyte YSZ, respectively, the of capacitances values being independent of temperature.

On the other hand, the range of low frequencies (LF) is distinguished by high capacitance values $C \approx 10^{-2}$ - 10^{-1} F. cm^{-2}, it is virtually independent of temperature, that means it's the same electrode phenomenon. L. Mogni *et al.* **[61]**, S. Pang *et al.* **[62]** and B. Philippeau *et. al.* **[14]** have attributed this contribution to the diffusion of O_2 gas through the porous electrode (*i.e.* electrode phenomena).

Relative to previous work **[20]**, increased capacity values (MF) have been observed, that can be linked to the presence of the interface layer between the electrode and the electrolyte. This increase in capacity values has been observed in the past, for example, by T. Ogier *et. al.* **[20]**, during the study of Ln_2NiO_4 materials (Ln: La, Pr or Nd) screen-printed on the YSZ electrolyte, covered with an interfacial layer of GDC. This range of capacitance is assigned to oxygen reduction response (ORR) processes, i.e. the phenomena of molecular dissociation of oxygen and charge transfer at the electrode/O_2 gas interface, instead of transfering ions to the electrode/layer interface **[45, 63, 64]**.

4. Conclusion

In the present work, $La_2NiO_{4,18}$, $La_2MnO_{4,13}$, $La_2CoO_{4,25}$ electrode materials were synthesized by the citrate route and thoroughly characterized by various techniques. With the aim of their possible use as oxygen electrode material for SOC cells, symmetrical half cells have been prepared. For this goal, commercial electrolyte $(ZrO_2)_{0,92}(Y_2O_3)_{0,08}$ (YSZ) was used and an interfacial layer based on YSZ (50%) + GDC(50%) added between the electrode materials and the electrolyte.

XPS analysis showed that the surface of the $La_2BO_{4\pm\delta}$ samples is rich in OH^- species providing its anionic character. This behavior can affect the phenomenon of oxygen diffusion at the surface of the samples also influencing the electrochemical behavior of the samples. In this

work, a positive behavior was observed in the case of the samples with an anionic **properties,** especially for L2NO and L2MO (**Table 4**).

According to the crystallographic results (XRD) and to the oxygen over-stoichiometry values, in the case of $La_2MnO_{4\pm\delta}$ whose cell is undistorted compared with those of $La_2NiO_{4\pm\delta}$ and $La_2CoO_{4\pm\delta}$ sample, it can be deduced that when the oxygen deficiency is low ($\delta < 0.15$) the interactions between anionic species are small, which improves the oxide ions migration. For the other materials, $La_2NiO_{4\pm\delta}$ and $La_2CoO_{4\pm\delta}$, the electronic conductivity becomes predominant.

The over-stoichiometry of oxygen (δ) varies from one material to another, probably due to the change in the state of the oxidation of the transition elements.

All cathode materials showed **favorable** chemical compatibility with the YSZ electrolyte in presence of the YSZ+GDC interfacial layer, under 1350 °C for at least 72 h.

From electrochemical measurements performed by EIS, low ASR values were observed for $La_2NiO_{4.18}$ in the presence of the interfacial layer (YSZ+GDC); these values are close to 0.43 Ω.cm^2 at 600 °C and 0.18 Ω.cm^2 at 700 °C, with an activation energy values of 0.72 eV. It can be concluded that the selected materials with the interfacial layer, except $La_2CoO_{4+\delta}$, exhibit good electrochemical properties at an intermediate temperature of 600 and 700 °C compared to similar materials without such a layer; this confirms the benefit of this new architecture. In this study, although the L2CO material exhibits the same anionic character as L2NO, but the high ASRs values were different, which is probably due to the poor electrical properties leading to poor electrochemical performance.

To conclude, the interest of structured cells constituted by an interface layer based on YSZ+GDC has been pointed out. These encouraging results suggest that $La_2NiO_{4.18}$ and $La_2MnO_{4.13}$ could be alternative cathode materials for IT-SOFCs.

5. References

[1] B. Zhu, Y. Mi, C. Xia, B. Wang, J. S. Kim, P. Lund, T. Li, A nanoscale perspective on solid oxide and semiconductor membrane fuel cells: Materials and technology: Energy Materials, 1 (2021), 100002.

[2] J. M. Bassat, M. Burriel, O. Wahyudi, R. Castaing, M. Ceretti, P. Veber, J. A. Kilner, Anisotropic oxygen diffusion properties in $Pr_2NiO_{4+\delta}$ and $Nd_2NiO_{4+\delta}$ single crystals: The Journal of Physical Chemistry C 117 (2013), 26466-26472.

[3] Y. Huan, S. Chen, R. Zeng, T. Wei, D. Dong, X. Hu and, Y, Huang, Intrinsic Effects of Ruddlesden-Popper-Based Bifunctional Catalysts for High-Temperature Oxygen Reduction and Evolution: Advanced Energy Materials 9 (2019), 1901573.

[4] I. D. Brown, Modelling the structures of La_2NiO_4: Zeitschrift für Cristallographie - Crystalline Materials, 199 (1992), 255-274.

[5] S. J. Skinner and J. A. Kilner, Oxygen diffusion and surface exchange in $La_{2-x}Sr_xNiO_{4+\delta}$: Solid State Ionics 135 (2000), 709-712.

[6] L. Minervini, R. W. Grimes, J. A. Kilner and K. E. Sickafus, Oxygen migration in $La_2NiO_{4+\delta}$: Journal of Materials Chemistry 10 (2000), 2349-2354.

[7] A. Montenegro-Hernandez, J. Vega-Castillo, L. Mogni, A. Caneiro, Thermal stability of $Ln_2NiO_{4+\delta}$ (Ln: La, Pr, Nd) and their chemical compatibility with YSZ and CGO solid electrolytes: International Journal of Hydrogen Energy 36 (2011), 15704-15714.

[8] S. Cho, Y. N. Kim, J. H. Kim, A. Manthiram, H. Wang, High power density thin film SOFCs with YSZ/GDC bilayer electrolyte: Electrochimica Acta 56 (2011), 5472–5477.

[9] I. Jang, S. Kim, C. Kim, H. Lee, H. Yoon, T. Song, U. Paik, Interface engineering of yttrium stabilized zirconia/gadolinium doped ceria bi-layer electrolyte solid oxide fuel cell for boosting electrochemical performance: Journal of Power Sources 435 (2019), 226776.

[10] D. Kim, K. T. Lee, Effect of lanthanide (Ln= La, Nd, and Pr) doping on electrochemical performance of $Ln_2NiO_{4+\delta}$ − YSZ composite cathodes for solid oxide fuel cells: Ceramics International 47 (2021), 2493-2498.

[11] V. N. Chaudhari, A. P. Khandale, S. S. Bhoga, An investigation on strontium doped $Sm_2NiO_{4+\delta}$ cathode for intermediate temperature solid oxide fuel cells: Journal of Power Sources 248 (2014), 647-654.

[12] S. Liping, H. Lihua, Z. Hui , L. Qiang , C. Pijolat, La substituted Sr_2MnO_4 as a possible cathode material in SOFC: Journal of Power Sources 179 (2008), 96–100.

[13] Y. Wang, H. Nie, S. Wang, T. L. Wen, U. Guth, V. Valshook, $A_{2-\alpha}A_{\alpha'}BO_4$-type oxides as cathode materials for IT-SOFCs (A=Pr, Sm; A′=Sr; B=Fe, Co): Materials Letters 60 (2006), 1174–1178.

[14] B. Philippeau, F. Mauvy, C. Mazataud, S. Fourcade, J. C. Grenier, Comparative study of electrochemical properties of mixed conducting $Ln_2NiO_{4+\delta}$ (Ln= La, Pr and Nd) and $La_{0.6}Sr_{0.4}Fe_{0.8}Co_{0.2}O_{3-\delta}$ as SOFC cathodes associated to $Ce_{0.9}Gd_{0.1}O_{2-\delta}$,$La_{0.8}Sr_{0.2}Ga_{0.8}Mg_{0.2}O_{3-\delta}$ and $La_9Sr_1Si_6O_{26.5}$ electrolytes: Solid State Ionics 249 (2013), 17-25.

[15] L. Lihua, G. Youbin, Z. Hua, J. Jiang, Electrochemical performance of La_2NiO_{4+d}–$La_{0.6}Sr_{0.4}Co_{0.2}Fe_{0.8}O_{3-d}$ composite cathodes for intermediate temperature solid oxide fuel cells: Materials Research Bulletin 45 (2010), 1135–1140.

[16] T. W. Chiu, Y. T. Lin, I. F. Yen, H. H. Hsieh, S. F. Wang, Properties and Performance of $La_2NiO_{4+\delta}$-$LaNiO_3$ Composite Cathodes for Intermediate-Temperature Solid Oxide Fuel Cells: Ferroelectrics, 457 (2013) , 105-110.

[17] C. Brahim, A. Ringuedé, E. Gourba, M. Cassir, A. Billard, P. Briois, Electrical properties of thin bilayered YSZ/GDC SOFC electrolyte elaborated by sputtering: Journal of Power Sources 156 (2006), 45–49.

[18] J. Kim, J. Kim, K. J. Yoon, J. W. Son, J. H. Lee, J. H. Lee, H- W. Lee, H.-Il Ji, Solid oxide fuel cells with zirconia/ceria bilayer electrolytes via roll calendering process: Journal of Alloys and Compounds 846 (2020), 156318.

[19] H. Mohebbi, S. M. Mirkazemi, Controlling Yttria-stabilized zirconia/gadolinia-doped ceria interdiffusion layer in the solid oxide fuel cell electrolyte via flash sintering method: Ionics 27 (2021), 5219–5227.

[20] T. Ogier, F. Mauvy, J. M. Bassat, J. Laurencin, J. Mougin, J. C. Grenier, Overstoichiometric oxides $Ln_2NiO_{4+\delta}$ (Ln = La, Pr or Nd) as oxygen anodic electrodes for solid oxide electrolysis application: International Journal of Hydrogen Energy 40 (2015) 15885–15892.

[21] S. Amira, M. Ferkhi, F. Mauvy, S. Fourcade, J.M. Bassat, J.C. Grenier, $La_{1.5}Nd_{0.3}Pr_{0.2}NiO_{4.16}$: A New Cathode Material for IT-Solid Oxide Fuel Cells, Electrocatalysis (2023), 1-15.

[22] M. Ferkhi, S. Khelili, L. Zerroual, A. Ringuedé, M. Cassir, Synthesis, structural analysis and electrochemical performance of low-copper content $La_2Ni_{1-x}Cu_xO_{4+\delta}$ materials as new cathodes for solid oxide fuel cells: Electrochim Acta 54 (2009), 6341–6346

[23] M. Ferkhi, A. Ringuede, A. Khaled, L. Zerroual, M. Cassir, $La_{1.98}NiO_{4\pm\delta}$, a new cathode material for solid oxide fuel cell: impedance spectroscopy study and compatibility with gadoliniadoped ceria and yttria-stabilized zirconia electrolytes: Electrochim Acta 75 (2012) 80–87.

[24] G. D. Christian, Analytical Chemistry, 5th edn., John Wiley &Sons Inc., New York, (1994) 284–383.

[25] X. Yang, X. Xu, S. Wu, S. Yu, L. Bi, Enhancing the performance of traditional La_2NiO_{4+x} cathode for proton-conducting solid oxide fuel cells with Zn-doping: Ceramics International 48 (2022), 19626-19632.

[26] J. Li, Z. Gao, H. Min, M. Li, Y. Lu, X. Wang, X. Ding. Enabled fast cathode kinetics for intermediate-temperature solid oxide fuel cell with improved CO_2 poisoning robustness: La_2NiO_4 surfaced-modified $SrCo_{0.8}Nb_{0.1}Ta_{0.1}O_{3-\delta}$ composite: Journal of Power Sources 506 (2021), 230057.

[27] M. Matsuda, M. Hashimoto, C. Matsunaga, T. S. Suzuki,Y. Sakka, T. Uchikoshi. Electrophoretic fabrication of a-b plane oriented La_2NiO_4 cathode onto electrolyte in strong magnetic field for low-temperature operating solid oxide fuel cell: Journal of the European Ceramic Society 36 (2016), 4077–4082.

[28] M. Hammad, B. Alkan, A. K. Al-kamal , C. Kim, M. Y. Ali, S. A,gel, H. T. A. Wiedemann, D. Klippert, T. C. Schmidt, C. W. M. Kay, H. Wiggers, Enhanced heterogeneous activation of peroxymonosulfate by Ruddlesden-Popper-type $La_2CoO_{4+\delta}$ nanoparticles for bisphenol A degradation: Chemical Engineering Journal 429 (2022), 131447.

[29] R. M. García de la Cruz, H. Falcón, M. A. Peña, J. L. G. Fierro, Role of bulk and surface structures of $La_{1-x}Sr_xNiO_3$ perovskite-type oxides in methane combustion: Applied Catalysis B: Environmental 33 (2001), 45-55.

[30] A. T. Fulmer, J. Dondlinger, M. A, Langell. Passivation of the La_2NiMnO_6 double perovskite to hydroxylation by excess nickel, and the fate of the hydroxylated surface upon heating: Applied surface science 305 (2014), 544-553.

[31] J. L. G. Fierro, Structure and composition of perovskite surface in relation to adsorption and catalytic properties: Catalysis Today 8 (1990), 153-174.

[32] J. L. G. Fierro, L, Gonzalez Tejuca. Non-stoichiometric surface behaviour of $LaMO_3$ oxides as evidenced by XPS: Applied surface science 27 (1987), 453-457.

[33] J. F. Moulder, W. F. Stickle, P. E. Sobol, K. D. Bomben, Handbook of X-ray photoelectron spectroscopy. Perkin-Elmer, Eden Prairie (1992) 44.

[34] C. D. Wagner, W. M. Riggs, L. E. Davis, J. F. Moulder, G. E. Muilenberg Handbook of Xray photoelectron spectroscopy. Perkin- Elmer, Physical Electronics Division, Eden Prairie (1976).

[35] S.Mickevičius, S.Grebinskij, V.Bondarenka, B.Vengalis, K.Šliužienė, B. A. Orlowski, V.Osinniy, W.Drube. Investigation of epitaxial $LaNiO_{3-x}$ thin films by highenergy XPSJournal of alloys and compounds 423 (2006), 107-111.

[36] A. Zine, M. Ferkhi, A. Khaled, E. K. Savan, $A_2BO_{4\pm\delta}$ as New Materials for Electrocatalytic Detection of Paracetamol and Diclofenac Drugs: Electrocatalysis 13 (2022), 524–538.

[37] H. W. Kang, S. N. Lim, S. B. Park, Co-doping schemes to enhance H_2 evolution under visible light irradiation over $SrTiO_3$: Ni/M (M= La or Ta) prepared by spray pyrolysis: International Journal of Hydrogen Energy 37 (2012), 5540-5549.

[38] M. Hammad, B. Alkan, A. K. Al-kamal, C. Kim, M. Y. Ali, S. Angel, H. T. A. Wiedemann, D. Klippert, T.C. Schmidt, C. W. M. Kay, H. Wiggers, Enhanced heterogeneous activation of peroxymonosulfate by Ruddlesden-Popper-type $La_2CoO_{4+\delta}$ nanoparticles for bisphenol A degradation: Chemical Engineering Journal, 429 (2022), 131447.

[39] J. Hu, L. Wang, L. Shi, H. Huang, Oxygen reduction reaction activity of $LaMn_{1-x}Co_xO_{3-\delta}$ graphene nanocomposite for zinc-air battery: Electrochimica Acta 161 (2015) 115-123.

[40] C. Zhang, W. Hua, C. Wang, Y. Guo, Y. Guo, G. Lu, A. Baylet, A. Giroir-Fendler, The effect of A-site substitution by Sr, Mg and Ce on the catalytic performance of $LaMnO_3$ catalysts for the oxidation of vinyl chloride emission: Appl. Catal. B 134 (2013), 310-315.

[41] Y. Wang, S. Xie, J. Deng, S. Deng, H. Wang, H. Yan, H. Dai, Morphologically controlled synthesis of porous spherical and cubic LaMnO3 with high activity for the catalytic removal of toluene: ACS Appl. Mater. Interfaces 6 (2014), 17394-17401.

[42] M. Burriel, S. Wilkins, J. P. Hill, M. A. Muñoz-Márquez, H. H. Brongersma, J. A. Kilner, M. P. Ryan and S. J. Skinner. Absence of Ni on the outer surface of Sr doped La_2NiO_4 single crystals, Energy Environ. Sci. 7 (2014), 311-316.

[43] M. Burriel, H. Téllez, R. J. Chater, R. Castaing, P. Veber, M. Zaghrioui, T. Ishihara, J. A. Kilner and J. M. Bassat. Influence of Crystal Orientation and Annealing on the Oxygen Diffusion and Surface Exchange of $La_2NiO_{4+\delta}$, J. Phys. Chem. 120 (2016) 17927–17938.

[44] M. L. Fontaine, C. Laberty-Robert, F. Ansart, P. Tailhades, Elaboration and characterization of $La_2NiO_{4+\delta}$ powders and thin films via a modified sol–gel process: Journal of Solid State Chemistry 177 (2004), 1471–1479.

[45] H. Zhao, F. Mauvy, C. Lalanne, J. M. Bassat, S. Fourcade, J. C. Grenier, New cathode materials for ITSOFC: Phase stability, oxygen exchange and cathode properties of $La_{2-x}NiO_{4+\delta}$: Solid State Ionics 179 (2008), 2000–2005.

[46] V**.** Vibhu, A. Rougier, C. Nicollet, A. Flura, J. C Grenier, J. M. Bassat, $La_{2-x}Pr_xNiO_{4+\delta}$ as suitable cathodes for metal supported SOFCs: Solid State Ionics 278 (2015) 32-37.

[47] E. Boehm, J. M. Bassat, M. C. Steil, P. Dordor, F. Mauvy, J. C. Grenier, Oxygen transport properties of $La_2Ni_{1-x}Cu_xO_{4+\delta}$ mixed conducting oxides: Solid State Sciences 5 (2003), 973–981.

[48] J. Dailly, S. Fourcade, A. Largeteau, F. Mauvy, J. C. Grenier, M. Marrony, Perovskite and A_2MO_4-type oxides as new cathode materials for protonic solid oxide fuel cells: Electrochimica Acta 55 (2010), 5847–5853.

[49] Q. Li, X. Zeng, L. Sun, H. Zhao, L. Huo, J. C. Grenier, Electrochemical performance of $La_2Cu_{1-x}Co_xO_4$ cathode materials for intermediate-temperature SOFCs: International journal of hydrogen energy 37 (2012), 2552-2558.

[50] R. Le Toquin, W. Paulus, A .Cousson, G. Dhalenne, A. Revcolevschi, Interstitial and apical oxygen order–disorder in $La_2CoO_{4+\delta}$ observed by single-crystal neutron and X-ray diffraction, Physica B: Condensed Matter 350 (2004), E269-E272.

[51] A. Nemudry, P. Rudolf, R. Schöllhorn, Room temperature topotactic oxidation of lanthanum cobalt oxide $La_2CoO_{4.0}$, Solid State Ionics 109 (1998), 213-222.

[52] A. Aguadero, J.A. Alonso and L. Daza. Oxygen Excess in La_2CoO_4: A Neutron Diffraction Study: Zeitschrift für Naturforschung 63b (2008), 615-622.

[53] N. M. Sammes , G. A. Tompsett, Z. Cai, The chemical reaction between ceria and fully stabilised zirconi: Solid State Ionics 121 (1999) 121–125.

[54] K. Eguchi , N. Akasaka, H. Mitsuyasu, Y. Nonaka, Process of solid state reaction between doped ceria and zirconia: Solid State Ionics 135 (2000), 589–594.

[55] D. Pérez-Coll, A. Aguadero, M. J. Escudero, P. Núñez, L. Daza, Optimization of the interface polarization of the La_2NiO_4-based cathode working with the $Ce_{1-x}Sm_xO_{2-\delta}$ electrolyte system: Journal of Power Sources 178 (2008) 151-162.

[56] P. Ramos-Alvarez,M. E. Villafuerte-Castrejón,G. González, M. Cassir, C. Flores Morales, J. A. Chávez-Carvayar. Ceria-based electrolytes with high surface area and improved conductivity for intermediate temperature solid oxide fuel cells: Journal of Materials Science 52 (2017), 519-532.

[57] W. S. Hsieh, P. Lin, S. F. Wang, Characteristics of electrolyte supported micro-tubular solid oxide fuel cells with GDC-ScSZ bilayer electrolyte: International Journal of hydrogen Energy 39 (2014), 17267-17274.

[58] M.J. Escudero, A. Aguadero, J. A. Alonso, L. Daza, A kinetic study of oxygen reduction reaction on La_2NiO_4 cathodes by means of impedance spectroscopy: Journal of Electroanalytical Chemistry 611 (2007), 107–116.

[59] R. J. Woolley, S. J. Skinner, Functionally graded composite $La_2NiO_{4+\delta}$ and $La_4Ni_3O_{10-\delta}$ solid oxide fuel cell cathodes: Solid State Ionics 255 (2014), 1–5.

[**60**] V. Vibhu, A. Rougier, C. Nicollet, A. Flura, J. C. Grenier and J. M. Bassat, $La_{2-x}Pr_xNiO_{4+\delta}$ as suitable cathodes for metal supported SOFCs: Solid State Ionics 278 (2015), 32-37.

[61] F. Mauvy, C. Lalanne, J. M. Bassat, J. C. Grenier, H. Zhao, P. Dordor, Ph.Stevens, Oxygen reduction on porous $La_2NiO_{4\pm\delta}$ electrodes: Journal of the European Ceramic Society 25 (2005), 2669–2672.

[62] J. Fondard, P. Bertrand, A. Billard, S. Fourcade, P. Batocchi, F. Mauvy, G. Bertrand, P. Briois, Manufacturing and testing of a metal supported Ni-YSZ/YSZ/La_2NiO_4 ITSOFC synthesized by physical surface deposition processes: Solid State Ionics 310 (2017), 10–23.

[63] M.Yousaf, M. Akbar, E. Hu, Y. Dong, M. N. Akhtar, M. Y. Shah, B. Zhu, Tuning ORR electrocatalytic functionalities in CGFO-GDC composite cathode for low-temperature solid oxide fuel cells: Ceramics International, 49 (2023), 6030-6038.

[64] M. Yousaf, M. Akbar, M.A.K.Y. Shah, A. Noor, Y. Lu, M. N. Akhtar, N. Mushtaq , E. Hu , S. Yan , B. Zhu, Enhanced ORR catalytic activity of rare earth-doped Gd oxide ions in a$CoFe_2O_4$ cathode for low-temperature solid oxide fuel cells (LT-SOFCs): Ceramics International 48 (2022),28142-28153.

[65] R. K. Sharma, S. K. Cheah, M. Burriel, L. Dessemond, J. M. Bassat and E. Djurado, Design of $La_{2-x}Pr_xNiO_{4+\delta}$ SOFC cathodes: a compromise between electrochemical performance and thermodynamic stability: Journal of Materials Chemistry A 5 (2017), 1120–1132.

[66] M. Rieu. Preparation by sol-gel route and characterization of a complete SOFC cell on a porous metal support (Doctoral dissertation 2009).

Table 1. Unit cell parameters and space group of L2NO, L2CO and L2MO samples.

Sample	Space Group	Unit cell parameters (Å)			Unit cell volume ($Å^3$)
		a	b	c	
L2NO	Fmmm	5.453 ± 0.001	5.469 ± 0.001	12.676 ± 0.002	378.0 ± 0.2
L2CO	Fmmm	5.555 ± 0.002	5.466 ± 0.001	12.651 ± 0.005	383.5 ± 0.3
L2MO	I4/mmm	3.858 ± 0.001	3.858 ± 0.001	12.953 ± 0.004	193.3 ± 0.2

Table 2. XPS calculated binding energies (eV) measured for the core-levels of L2NO, L2CO and L2MO materials. B: Ni, Co or Mn.

Sample	O1s	Main peak positions (eV)		B^{3+}/B^{2+} or B^{4+}/B^{3+}
L2NO	**1)** 528.69 (27.5) **2)** 530.17 (11.8) **3)** 531.45 (57.2) **4)** 533.22 (03.4)	**La3d$_{3/2}$** **849.94** **851.58**	**Ni 2p$_{3/2}$** **854.43** **855.73**	0.34
L2CO	**1)** 528.56 (09.6) **2)** 530.43 (15.3) **3)** 531.36 (50.6) **4)** 532.47 (20.9) **5)** 533.76 (03.4)	**Co 2p$_{3/2}$** **779.14** **780.60**	**Co 2p$_{1/2}$** **794.58** **796.39**	0.42
L2MO	**1)** 528.72 (21.2) **2)** 530.65 (39.0) **3)** 531.42 (33.9) **4)** 532.96 (05.9)	**Mn 2p$_{3/2}$** **641.12** **642.61**	**Mn 2p$_{1/2}$** **652.69** **655.49**	0.55

Table 3. Atomic ratios of elements for L2NO, L2CO and L2MO materials as determined by XPS. B: Ni, Co or Mn.

Sample	$\frac{\mathbf{La}}{\mathbf{B}}$	$\mathbf{O_{ads\ (M-OH)}}\%$	$\frac{\mathbf{O_{latt}}}{\sum \mathbf{cations}}$	$\frac{\mathbf{O_{ads\ (M-OH)}}}{\mathbf{O_{latt}}}$
L2NO	4.60	27.5	1.70	1.26
L2CO	4.07	19.82	1.66	1.65
L2MO	5.84	11.36	1.70	0.37

Table 4. ASRs values and activation energies for oxygen electrode materials layered on YSZ electrolyte in presence of YSZ+GDC interlayer (this work) compared with those reported in the literature. * Interfacial layer

Symmetrical cell	Rp (Ω.cm²)/T (°C)	Ea (eV)	Ref. Year
On YSZ electrolyte			
La_2NiO_4 / **8YSZ**	0.53/700 °C	-	**[59], 2014**
La_2NiO_4 / **8YSZ**	0.37/ 800 °C	1.40	**[20], 2015**
La_2NiO_4 / **8YSZ**	0.93/ 600 °C	-	**[60], 2015**
La_2NiO_4 / **8YSZ**	2.55/800 °C		**[61], 2005**
La_2NiO_4 / **8YSZ**	4.00/800 °C		**[58], 2007**
La_2NiO_4/***GDC****/ **8YSZ**	3.06/700 °C	-	**[62], 2017**
$La_{0.5}Pr_{1.5}NiO_4$ / **8YSZ**	0.230/600 °C	-	**[36], 2015**
$LaPrNiO_4$ / **8YSZ**	0.290/600 °C	-	**[36], 2015**
$Pr_2NiO_{4+\delta}$ / **8YSZ**	0.150/600 °C	-	**[36], 2015**
$Pr_2NiO_{4+\delta}$ / **8YSZ**	0.20/700 °C	0.90	**[46], 2015**
$Nd_2NiO_{4+\delta}$ /**8YSZ**	0.50/700 °C	1.27	**[46], 2015**
La_2NiO_4 / **8YSZ**	2.00/700 °C	1.53	**[46], 2015**
$Pr_2NiO_{4+\delta}$ /$\mathbf{Ce_{0.8}Gd_{0.2}O_{2-\delta}}$*/ **8YSZ**	0.05/800 °C	-	**[18], 2015**
$Nd_2NiO_{4+\delta}$ /$\mathbf{Ce_{0.8}Gd_{0.2}O_{2-\delta}}$*/**8YSZ**	0.09/800 °C	-	**[18], 2015**
$La_2NiO_{4+\delta}$/ **YSZ+GDC*/YSZ**	0.43/600 °C, 0.18/700 °C	0.72	**This work**
$La_2MnO_{4+\delta}$/ **YSZ+GDC*/YSZ**	2.44/600 °C, 01.80/700 °C	1,08	**This work**
$La_2CoO_{4+\delta}$/ **YSZ+GDC*/YSZ**	61.9/600 °C, 11.0 /700 °C	0.92	**This work**

Figures Caption

Fig. 1. Scheme of the symmetric cell: L2MO/ (YSZ+GDC)/YSZ/(YSZ+GDC)/L2MO.

Fig. 2. XRD of the: **a)** L2NO, **b)** L2CO and **c)** L2MO powders.

Fig. 3. Curve fitting of the O1s and (Ni, Co and Mn)2p core levels XPS signals of:

a) and **b)**: L2MO, **c)** and **d):** L2CO, **e)** and **f):** L2NO.

Fig. 4. SEM images of the synthesized materials: **a)** L2NO, **b)** L2CO, **c)** L2MO after sintering at 1000 °C for **4 h.**

Fig. 5. Cross-section images of symmetrical cell: Cathode / Interfacial layer / Electrolyte / Interfacial layer / Cathode.

Fig. 6. XRD diagrams of IL: YSZ (50%) + GDC (50%) after heating at 1350 °C during 3 days.

Fig. 7. XRD diagrams of YSZ (50%) + GDC (50%) /GDC and YSZ (50%) + GDC (50%) /YSZ after heating to 1350 °C during 3 days.

Fig. 8. XRD diagrams of the cathode material L2NO / 8YSZ + GDC mixture after heating at 1000 °C for 3 days.

Fig. 9. Typical Nyquist diagram corresponding to YSZ pellet.

Fig. 10. Arrhenius diagrams of the ionic conductivity of YSZ electrolyte in air ; our data (black dots); for comparison, the results found by Philippeau *et. al* [9] are reported in blue color)**.**

Fig. 11. Nyquist diagrams of the symmetrical cell IL:(YSZ+GDC) /YSZ in air, at 300, 400 and 700 °C.

Fig. 12. Arrhenius diagrams of the ionic conductivity of the whole interfacial layer deposited on the YSZ electrolyte compared with YSZ and GDC electrolytes.

Fig. 13. Nyquist diagrams of the symmetrical L2NO / (YSZ + GDC) / YSZ cell in air, at 300, 500 and 700 °C.

Fig. 14. Arrhenius plots of the Area Specific Resistances (ASR) of the L2NO, L2MO and L2CO cathode materials on the YSZ electrolyte in the presence of the interfacial layer (YSZ + GDC).

Fig. 15. Arrhenius diagrams: capacitance of the L2NO, L2MO and L2CO cathode materials deposited on YSZ electrolyte with YSZ+GDC interfacial layer.

Fig. 1.

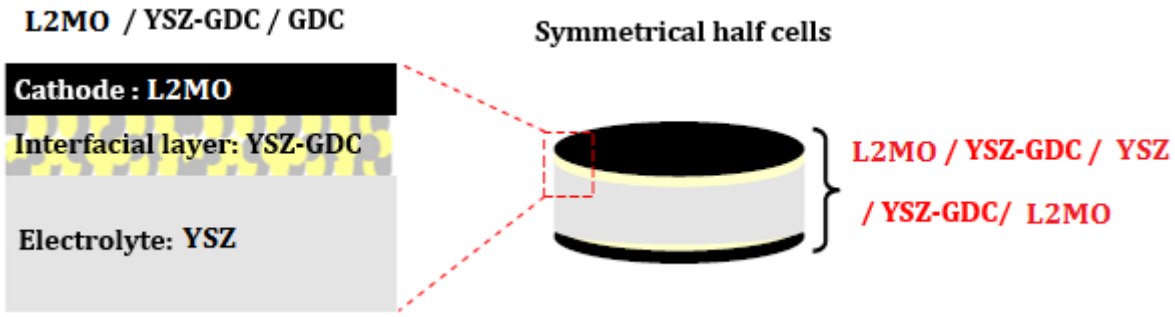
L2MO / YSZ-GDC / GDC
Cathode : L2MO
Interfacial layer: YSZ-GDC
Electrolyte: YSZ
Symmetrical half cells
L2MO / YSZ-GDC / YSZ
/ YSZ-GDC/ L2MO

Fig. 2.

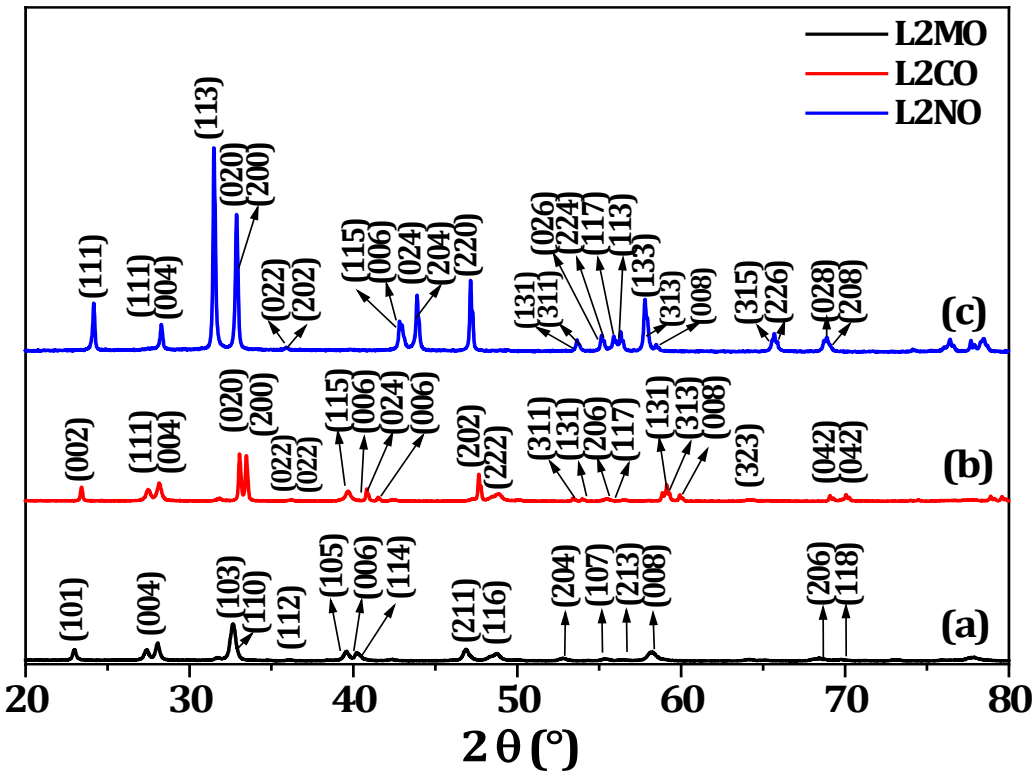
L2MO
L2CO
L2NO
(c)
(b)
(a)
2 θ (°)
20
30
40
50
60
70
80
(111)
(111)
(004)
(113)
(020)
(200)
(022)
(202)
(115)
(006)
(024)
(204)
(220)
(131)
(311)
(026)
(224)
(117)
(113)
(133)
(313)
(008)
(315)
(226)
(028)
(208)
(002)
(111)
(004)
(020)
(200)
(022)
(022)
(115)
(006)
(024)
(006)
(202)
(222)
(311)
(131)
(206)
(117)
(131)
(313)
(008)
(323)
(042)
(042)
(101)
(004)
(103)
(110)
(112)
(105)
(006)
(114)
(211)
(116)
(204)
(107)
(213)
(008)
(206)
(118)

Fig. 3.

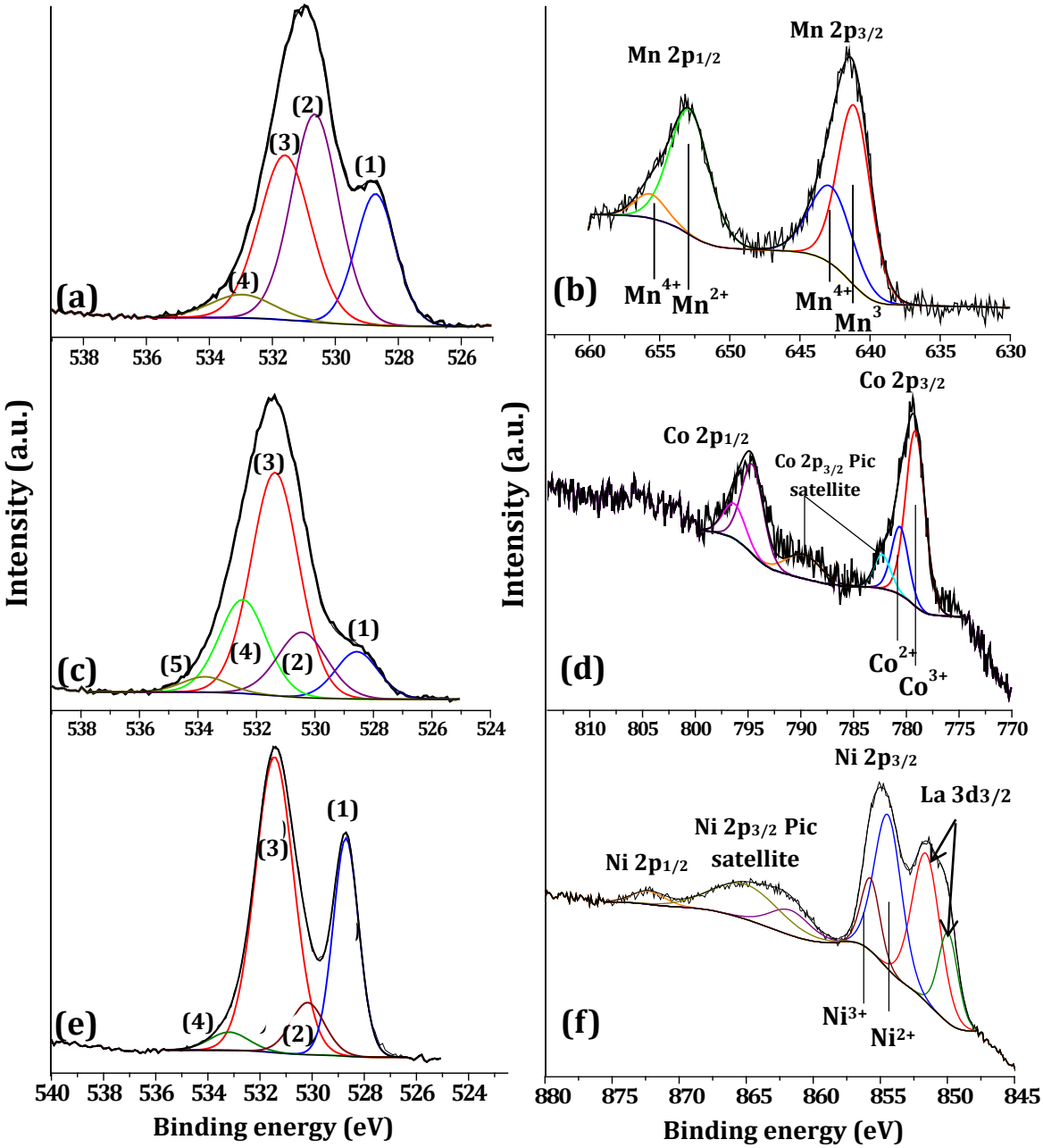
(a)
(1)
(2)
(3)
(4)
538 536 534 532 530 528 526
(b)
Mn 2p1/2
Mn 2p3/2
Mn4+
Mn2+
Mn4+
Mn3
660 655 650 645 640 635 630
(c)
(1)
(2)
(3)
(4)
(5)
538 536 534 532 530 528 526 524
(d)
Co 2p3/2
Co 2p1/2
Co 2p3/2 Pic satellite
Co2+
Co3+
810 805 800 795 790 785 780 775 770
(e)
(1)
(2)
(3)
(4)
540 538 536 534 532 530 528 526 524
(f)
Ni 2p3/2
La 3d3/2
Ni 2p3/2 Pic satellite
Ni 2p1/2
Ni3+
Ni2+
880 875 870 865 860 855 850 845
Intensity (a.u.)
Intensity (a.u.)
Binding energy (eV)
Binding energy (eV)

Fig. 4.

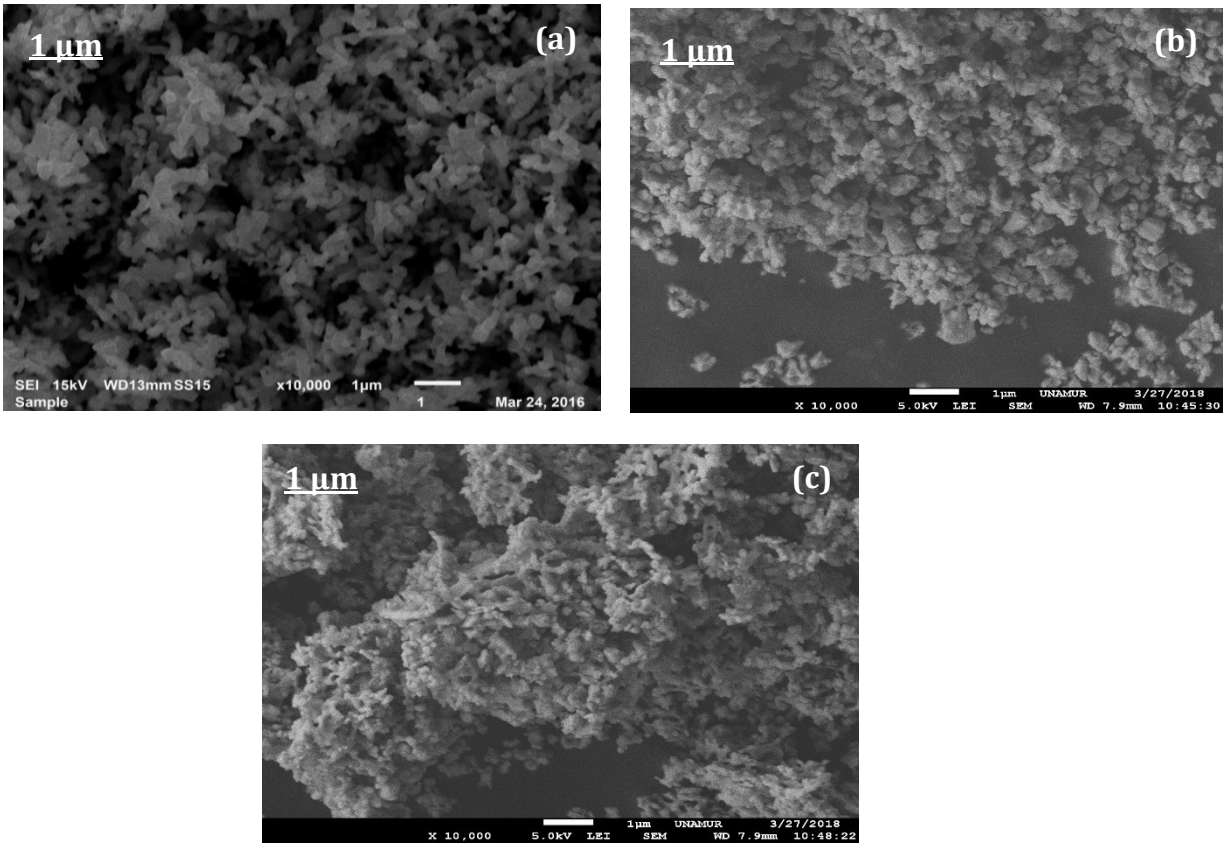
1 µm
(a)
SEI 15kV WD13mm SS15 x10,000 1µm
Sample
1
Mar 24, 2016
1 µm
(b)
1µm UNAMUR 3/27/2018
X 10,000 5.0kV LEI SEM WD 7.9mm 10:45:30
1 µm
(c)
1µm UNAMUR 3/27/2018
X 10,000 5.0kV LEI SEM WD 7.9mm 10:48:22

Fig. 5.

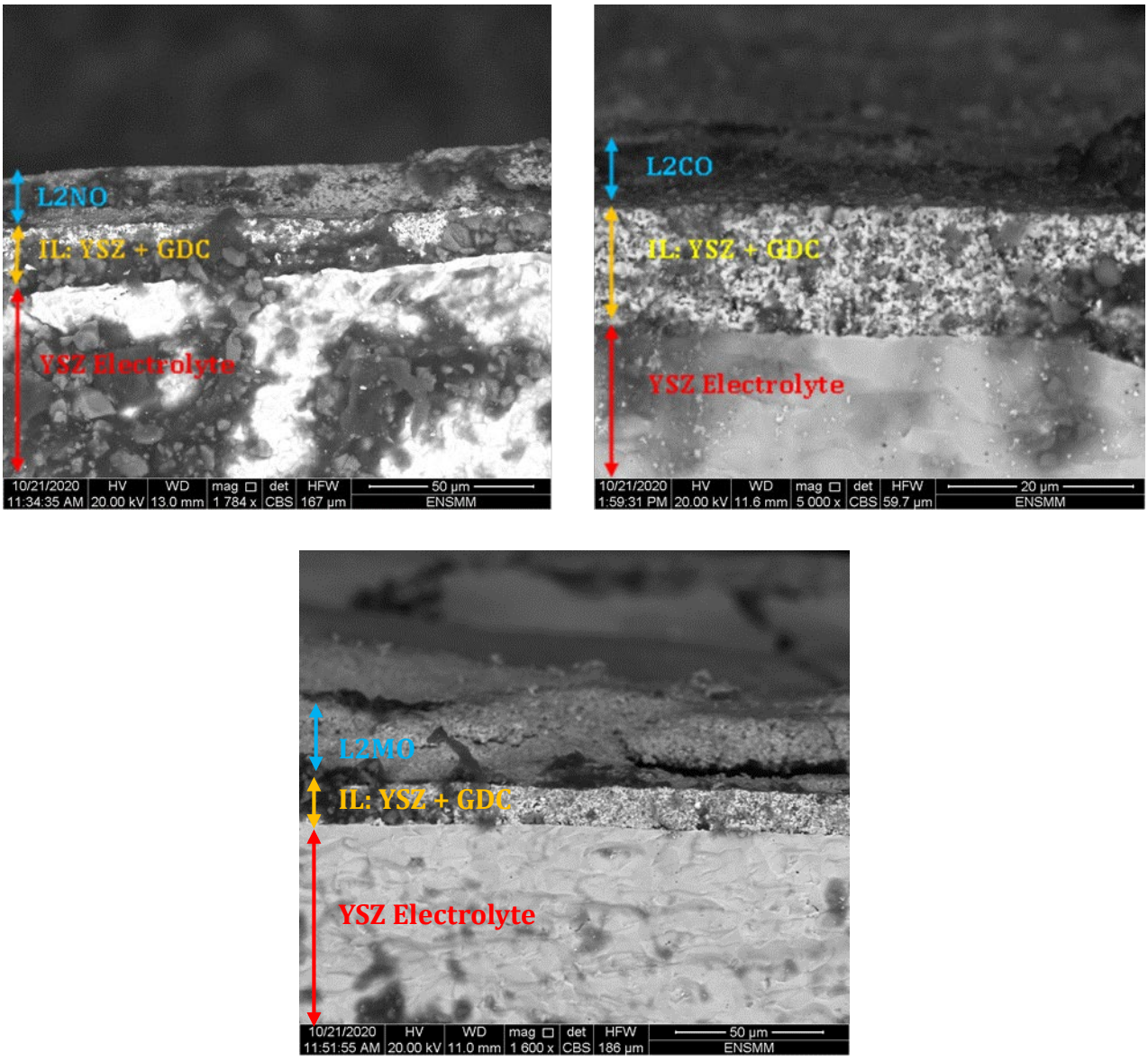
L2NO
IL: YSZ + GDC
YSZ Electrolyte
10/21/2020 11:34:35 AM
HV 20.00 kV
WD 13.0 mm
mag 1 784 x
det CBS
HFW 167 µm
50 µm
ENSMM
L2CO
IL: YSZ + GDC
YSZ Electrolyte
10/21/2020 1:59:31 PM
HV 20.00 kV
WD 11.6 mm
mag 5 000 x
det CBS
HFW 59.7 µm
20 µm
ENSMM
L2MO
IL: YSZ + GDC
YSZ Electrolyte
10/21/2020 11:51:55 AM
HV 20.00 kV
WD 11.0 mm
mag 1 600 x
det CBS
HFW 186 µm
50 µm
ENSMM

Fig. 6.

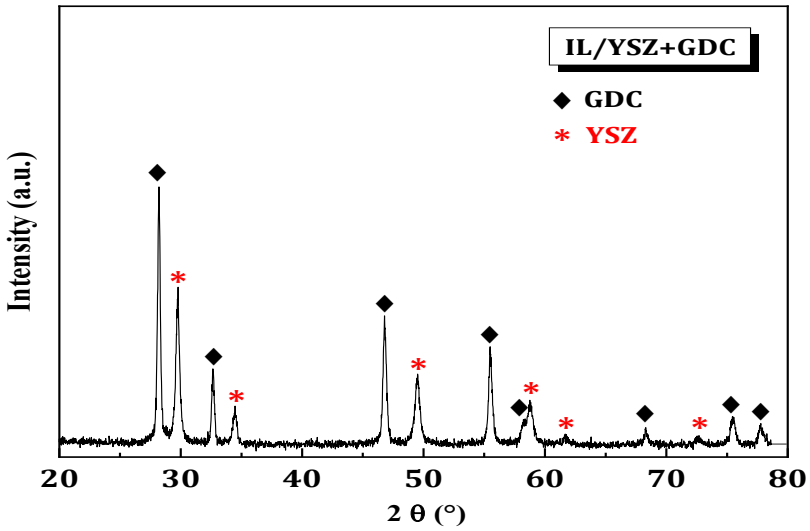

Fig. 7.

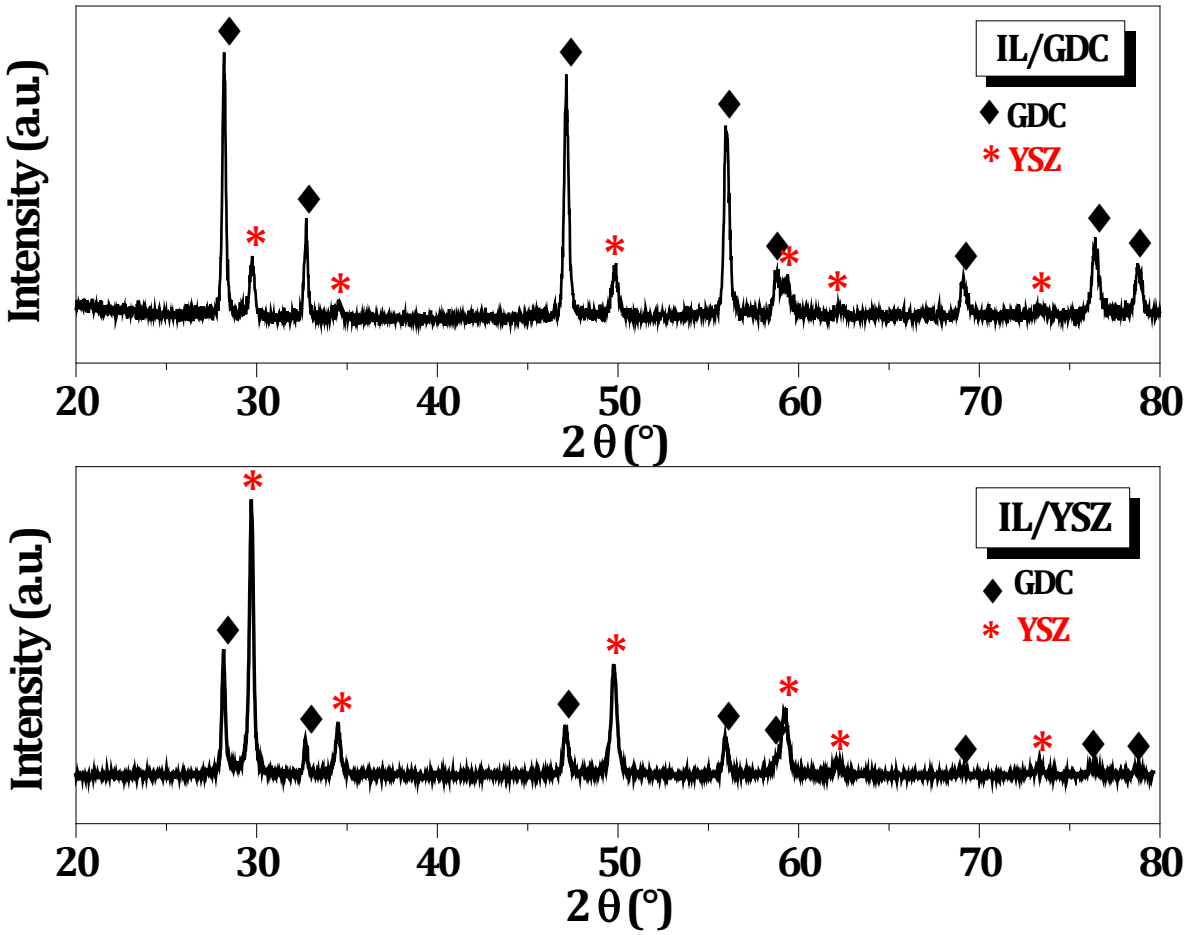
IL/GDC
GDC
YSZ
Intensity (a.u.)
20
30
40
50
60
70
80
2θ (°)
IL/YSZ
GDC
YSZ
Intensity (a.u.)
20
30
40
50
60
70
80
2θ (°)

Fig. 8.

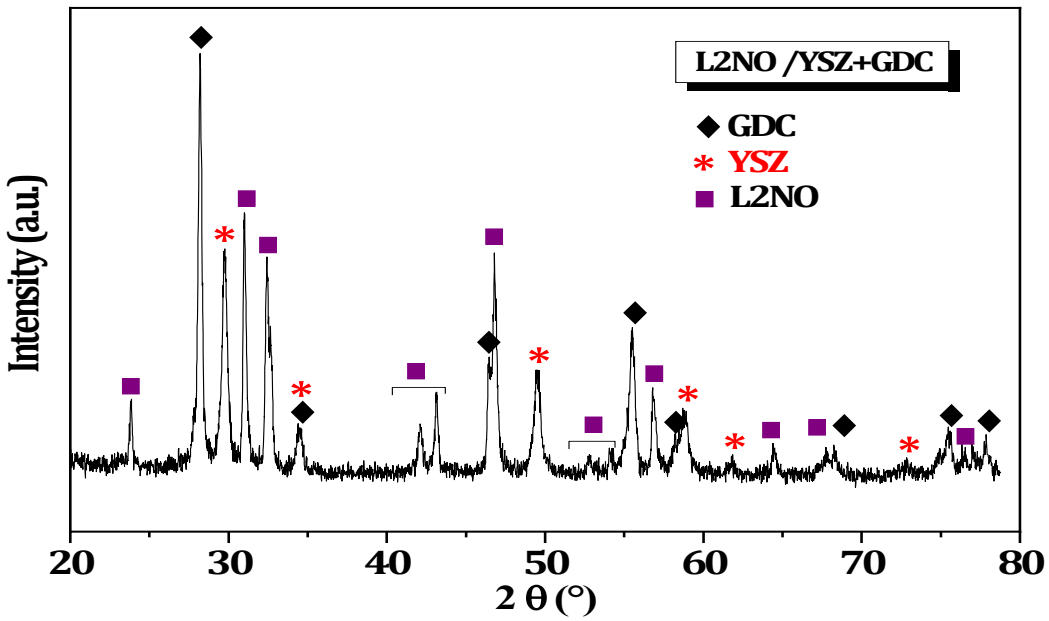

Fig. 9.

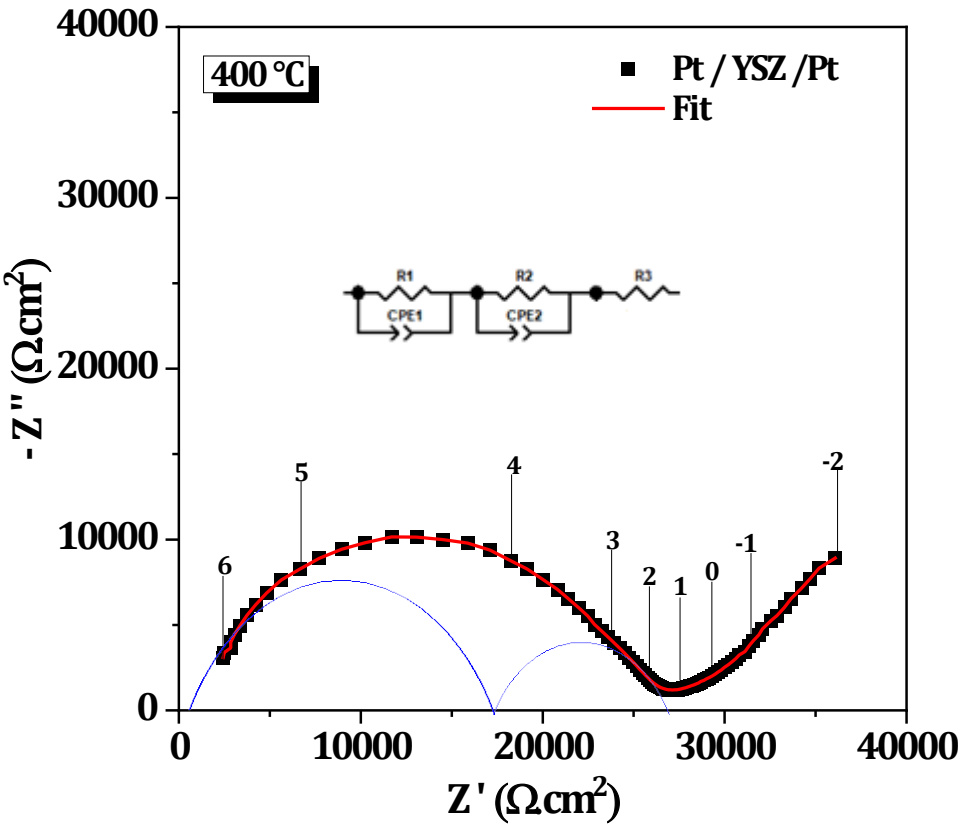
400 °C
Pt / YSZ /Pt
Fit
R1
R2
R3
CPE1
CPE2
-Z'' (Ωcm²)
Z' (Ωcm²)
0
10000
20000
30000
40000
6
5
4
3
2
1
0
-1
-2

Fig. 10.

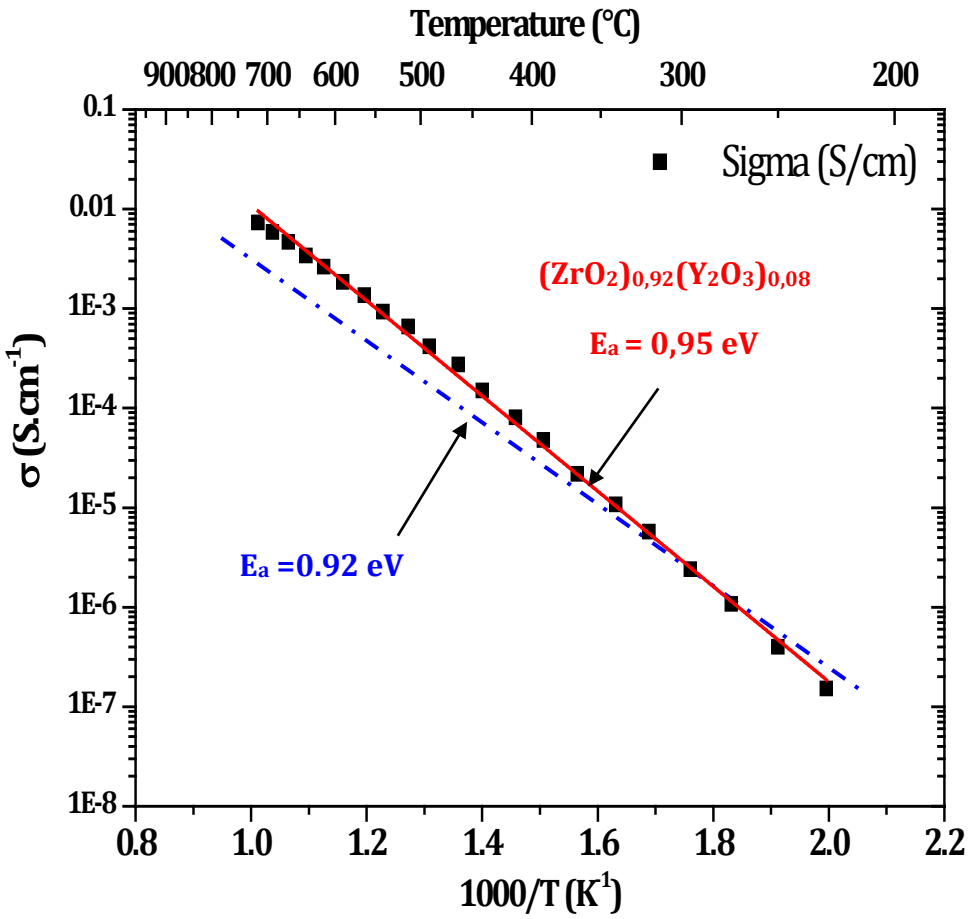
Temperature (°C)
900800 700 600 500 400 300 200
0.1
0.01
1E-3
1E-4
1E-5
1E-6
1E-7
1E-8
σ (S.cm-1)
Sigma (S/cm)
(ZrO2)0,92(Y2O3)0,08
Ea = 0,95 eV
Ea =0.92 eV
0.8 1.0 1.2 1.4 1.6 1.8 2.0 2.2
1000/T (K-1)

Fig. 11.

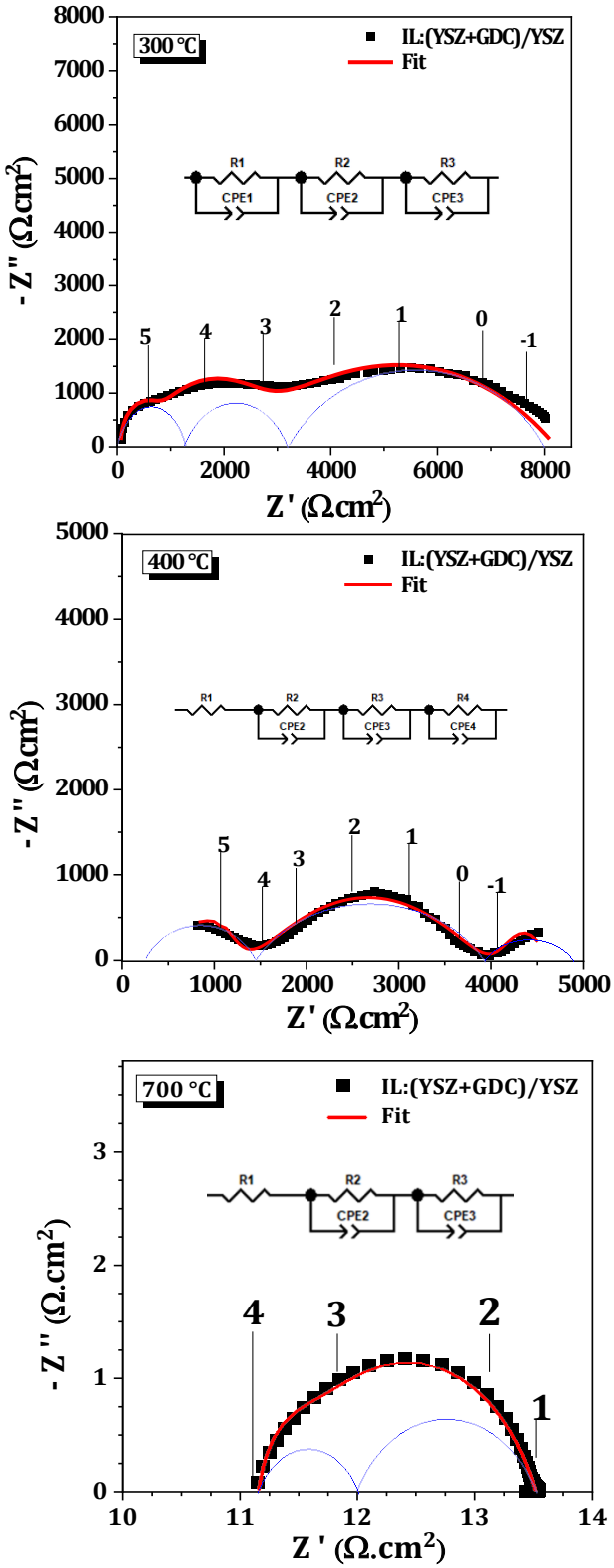
300 °C
IL:(YSZ+GDC)/YSZ
Fit
R1
R2
R3
CPE1
CPE2
CPE3
-Z'' (Ωcm²)
Z' (Ωcm²)
5
4
3
2
1
0
-1
400 °C
IL:(YSZ+GDC)/YSZ
Fit
R1
R2
R3
R4
CPE2
CPE3
CPE4
-Z'' (Ωcm²)
Z' (Ωcm²)
700 °C
IL:(YSZ+GDC)/YSZ
Fit
R1
R2
R3
CPE2
CPE3
-Z'' (Ω.cm²)
Z' (Ω.cm²)

Fig. 12.

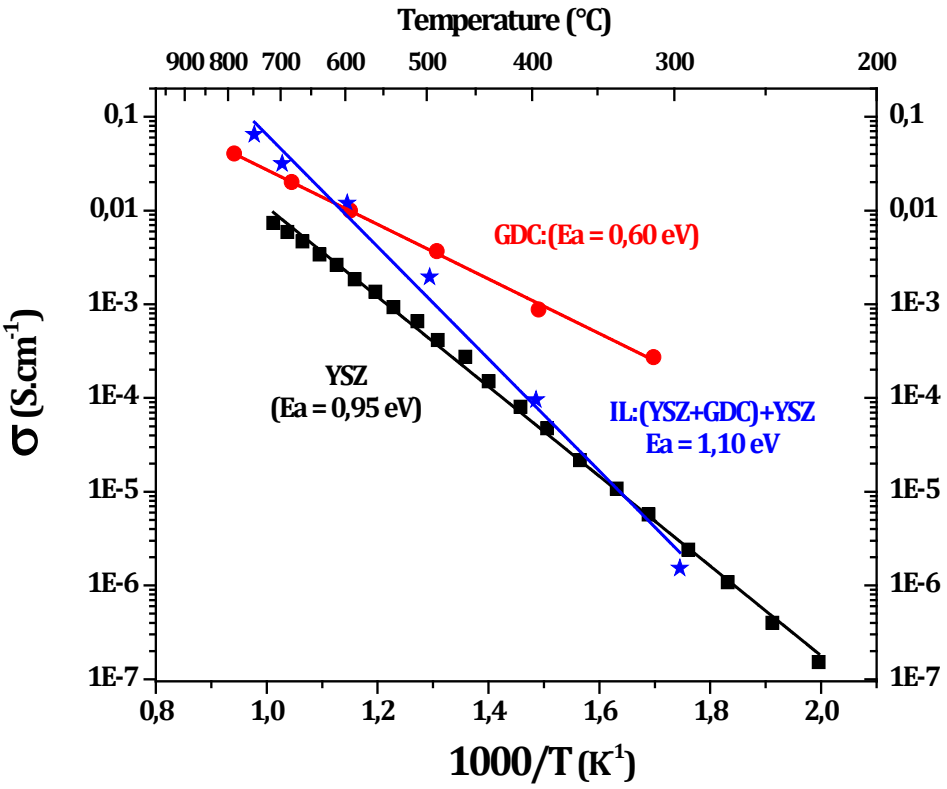
Temperature (°C)
900 800 700 600 500 400 300 200
0,1
0,01
1E-3
1E-4
1E-5
1E-6
1E-7
σ (S.cm-1)
GDC:(Ea = 0,60 eV)
YSZ
(Ea = 0,95 eV)
IL:(YSZ+GDC)+YSZ
Ea = 1,10 eV
0,8 1,0 1,2 1,4 1,6 1,8 2,0
1000/T (K-1)

Fig. 13.

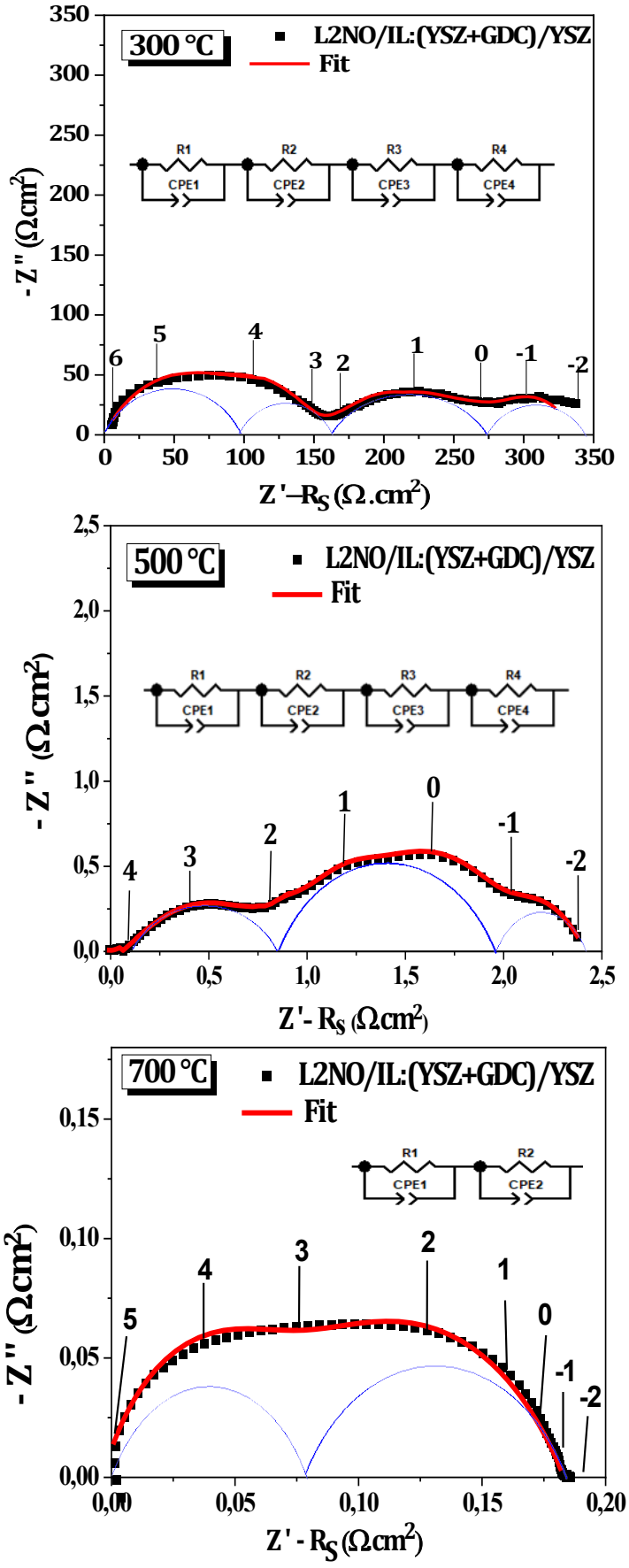
300 °C
L2NO/IL:(YSZ+GDC)/YSZ
Fit
R1
R2
R3
R4
CPE1
CPE2
CPE3
CPE4
- Z'' (Ωcm²)
Z' – Rs (Ω.cm²)
500 °C
L2NO/IL:(YSZ+GDC)/YSZ
Fit
- Z'' (Ωcm²)
Z' - Rs (Ωcm²)
700 °C
L2NO/IL:(YSZ+GDC)/YSZ
Fit
- Z'' (Ωcm²)
Z' - Rs (Ωcm²)

Fig. 14.

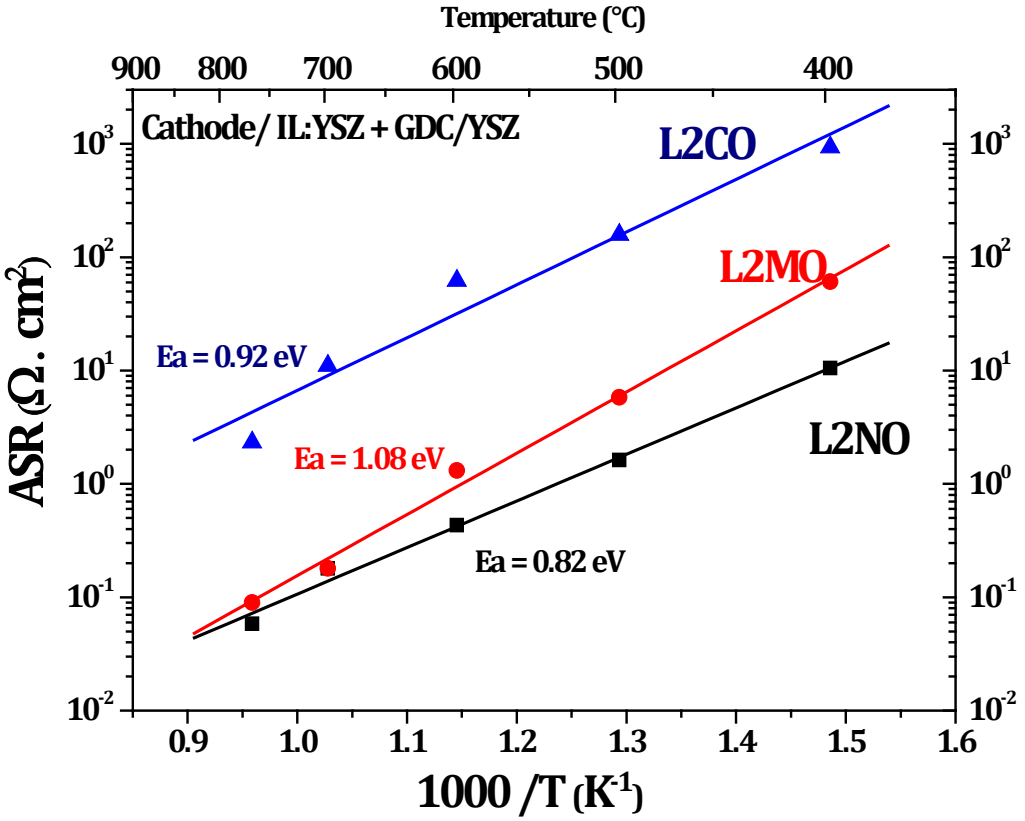
Temperature (°C)
900
800
700
600
500
400
Cathode/ IL:YSZ + GDC/YSZ
L2CO
L2MO
L2NO
Ea = 0.92 eV
Ea = 1.08 eV
Ea = 0.82 eV
ASR (Ω. cm²)
1000 /T (K⁻¹)
0.9
1.0
1.1
1.2
1.3
1.4
1.5
1.6

Fig. 15.

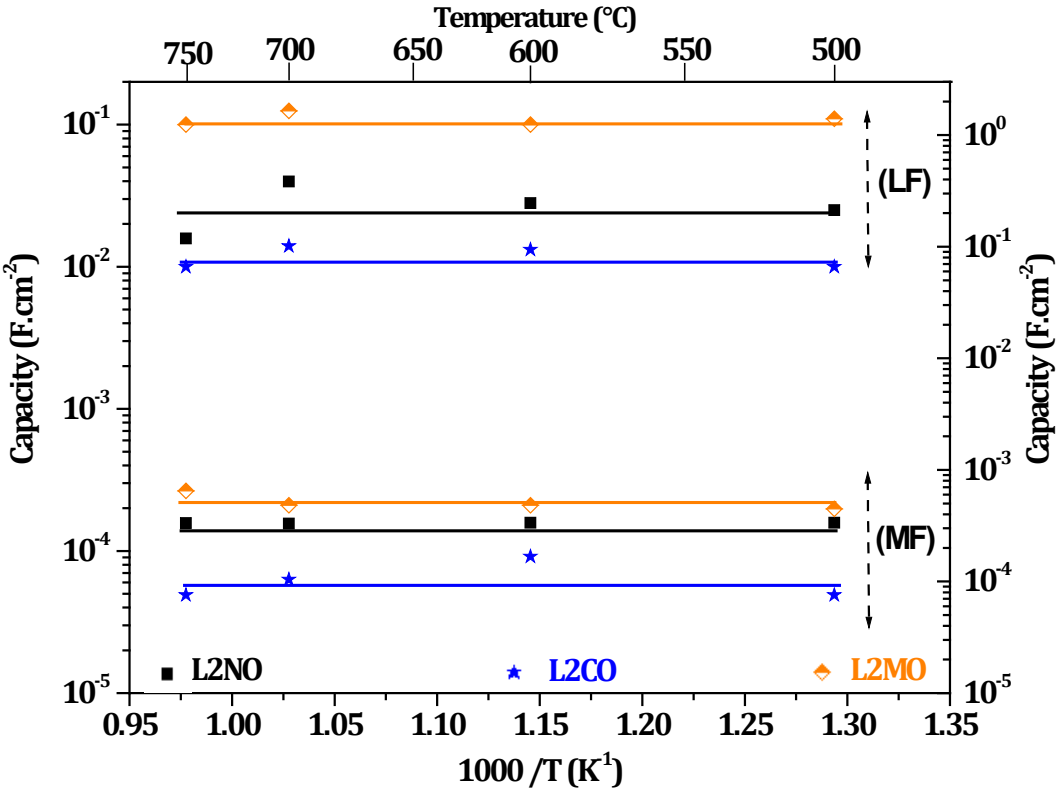
Temperature (°C)
750
700
650
600
550
500
Capacity (F.cm-2)
10-1
10-2
10-3
10-4
10-5
100
10-1
10-2
10-3
10-4
10-5
(LF)
(MF)
L2NO
L2CO
L2MO
0.95
1.00
1.05
1.10
1.15
1.20
1.25
1.30
1.35
1000 /T (K-1)

Table. SI1. Oxygen over-stoichiometry values determined at 25 °C for the as-prepared A_2BO_4 compounds.

Sample	**Over-stoichiometry (δ_{iod})**
L2NO	0.177
L2CO	0.248
L2MO	0.130